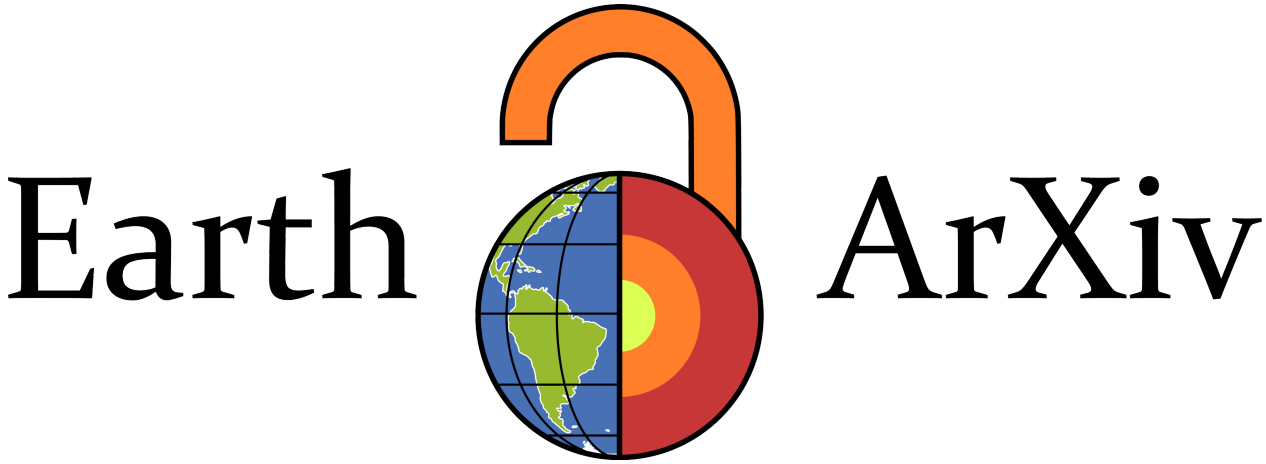

Low-cost autonomous chambers enable high spatial and temporal resolution monitoring of soil CO_2 exchange across landscapes

Authors: Jonathan Gewirtzman[1*], Ashley Keiser[2], Matthew A. Nieland[2], Corey Palmer[2], Vatsal Patel[3], Kelly Caylor[4], Elizabeth Forbes[1,5*]

[1] Yale School of the Environment, Yale University, New Haven, CT
[2] Stockbridge School of Agriculture, University of Massachusetts Amherst, Amherst, Massachusetts
[3] School of Engineering and Applied Science, Yale University, New Haven, CT
[4] Bren School of Environmental Science and Management, University of California Santa Barbara, Santa Barbara, CA
[5] Hudson Carbon, Hudson, NY
* Corresponding authors: jonathan.gewirtzman@yale.edu, eforbes@hudsoncarbon.com

Abstract

1. Soil CO_2 flux is a critical component of ecosystem carbon cycling, but due to high cost and mechanistic constraints, existing measurement systems are often limited by trade-offs between resolution (temporal and spatial), and spatial coverage. These constraints hinder efforts to monitor soil fluxes across diverse, heterogeneous landscapes and environmental gradients.
2. We developed Fluxbot 2.0, a low-cost, autonomous chamber system capable of continuous, distributed soil CO_2 flux measurements without external power or infrastructure. To assess its capability to capture landscape-scale variability, we deployed two Fluxbot 2.0 arrays, one at each of two hemlock forest sites in Harvard Forest, Massachusetts, USA, and compared its estimates of flux to those from existing, well-established automated chamber arrays that rely on multiplexed chambers and high-accuracy CO_2 analyzer units.
3. Fluxbots successfully captured site means, spatial variability, temporal patterns, and environmental responses, including temperature-driven flux dynamics. These measurements reflected differences in forest conditions between two sites and showed that distributed arrays of low-cost sensors can effectively capture both fine-scale variability and broader patterns across a landscape.
4. By enabling low-cost, autonomous monitoring of soil carbon flux in strategically distributed arrays, Fluxbot 2.0 addresses key gaps in existing soil CO_2 flux datasets. The system facilitates measurements across environmental gradients and heterogeneous landscapes, supporting research on soil carbon dynamics and biotic interactions that influence carbon cycling.

1. Introduction

Soil respiration, hereafter soil carbon (C) flux, is the largest terrestrial source of carbon dioxide (CO_2) to the atmosphere, accounting for over 90 Pg C annually (Bond-Lamberty and Thomson 2010; Hashimoto et al. 2023), the majority of gross terrestrial ecosystem emissions (Friedlingstein et al. 2025). It is an essential component of accurate ecosystem carbon budgets, allowing researchers to describe fluxes and feedbacks between terrestrial ecosystems and the atmosphere. Soil CO_2 flux is significantly variable across temporal scales (from diurnal to seasonal), spatial scales (from centimeters to kilometers) (Vargas et al. 2011; Bradford and Ryan 2008), and across topography, vegetation, and disturbance patterns (Rodeghiero and Cescatti 2008), requiring high spatial and temporal resolution as well as broad spatial coverage in data collection to characterize accurately.

Recent studies highlight how landscape heterogeneity across scales from centimeters to kilometers fundamentally influences C fluxes (Premke et al. 2016). Factors like microtopography, individual plant species, and species assemblages create localized element cycling hotspots, requiring high resolution monitoring (Jevon et al. 2023; Keiser et al. 2024). Spatial variability and temporal fluctuation in soil moisture and chemistry can lead to hot spots and hot moments of soil fluxes in natural environments (Gachibu et al. 2023; Leon et al. 2014; Savage et al. 2014). Land use change through urbanization and ecosystem fragmentation can influence spatial patterns in soil CO_2 flux across overlapping gradients with additive or synergistic effects (Garvey et al. 2022; Reinmann et al. 2020). Fauna, from small soil dwellers to megafaunal ecosystem engineers, can further induce spatial heterogeneity. Animals, both wild (e.g., Ohashi et al. 2007; Saunders et al. 2023) and domestic (e.g., Ondier et al. 2020), and changes to those communities (Forbes et al. 2019) require spatially distributed and/or spatially dense measurements to capture species' heterogeneous effects on soil C cycling across scales (DeCarlo and Caylor 2019; Ferraro and Lienau 2025; Schmitz et al. 2018; Risch et al. 2013).

Through time, these processes vary and are modulated by daily cycles in edaphic conditions (e.g. (Forbes et al. 2023; Tang et al. 2005; Savage et al. 2009; Huang et al. 2020; Savage et al. 2014)), seasonal change (Giasson et al. 2013; Davidson et al. 2006) , and changing climate (Raich et al. 2002; Carey et al. 2016). Beyond its utility for parsing ecologically-specific questions, high-resolution soil carbon flux monitoring also supports data-driven approaches for carbon offset projects and credit programs in contexts like agroecology (Kim et al. 2025; Paustian et al. 1997; Paustian et al. 2000; Paustian et al. 2016), which would move efforts away from current estimation-based methods (Novick et al. 2022).

To capture variability in soil carbon flux, researchers use a range of gas analysis methods and associated tools. Hand-held, manually-operated "survey" chambers with precision gas analyzers can capture detailed spatial patterns in soil CO_2 flux through distributed sampling, but due to cost and labor constraints provide limited temporal resolution or reliable comparisons

across large spatial extents. Commercial automated chambers provide excellent temporal resolution but are prohibitively expensive (often >$20,000 USD per system), limiting deployments to small numbers of chambers at single locations (Savage and Davidson 2003). Eddy covariance towers monitor ecosystem-scale fluxes with high temporal resolution and large spatial extents, but lack spatial resolution needed to identify specific drivers of flux variability (Hollinger et al. 2004) . In all cases, logistical constraints prevent researchers from asking questions that interrogate high spatial resolution, temporal resolution, and spatial scale simultaneously (Forbes et al. 2023; Pan et al. 2024).

While measurement precision and instrument durability are important considerations, soil CO_2 flux monitoring objectives may benefit from trading some precision for greatly expanded coverage through distributed arrays of autonomous devices. Advances in low-cost CO_2 sensors enable new approaches to ecosystem gas exchange data collection centered around replication (Pereira and Ramos 2022). Building on our previous work developing the original Fluxbot—a low-cost, autonomous soil CO_2 flux chamber system (Forbes et al. 2023; Pan et al. 2024)—we present here the first landscape-scale validation of a low-cost, automated and near-continuous array of Fluxbot 2.0 autochambers. Fluxbot 2.0 aims to further address key data gaps with capabilities that enable more access to high-resolution soil CO_2 flux monitoring across heterogeneous contexts.

We validated two distributed arrays of Fluxbot 2.0 and directly compared their outputs with those from two established arrays of automated flux chambers at the Harvard Forest, where multiplexed automated chambers (or, autochambers) coupled to traditional high-precision flow-through infra-red gas analyzers (IRGA) have been continuously monitoring soil CO_2 flux in contrasting forest stands for over a decade. We assess the performance of Fluxbot 2.0 relative to the established autochambers under field conditions, demonstrating their scalability and ability to accurately detect fluxes across spatially heterogeneous and dispersed locations.

2. Methods

We worked in two eastern hemlock (*Tsuga canadensis* L.) forest stands approximately 1.4 km apart at the Harvard Forest Long Term Ecological Research (LTER) Site in Petersham, Massachusetts, USA. The two stands, located at 42.541500, -72.174624 (stand 1) and 42.529162, -72.178581 (stand 2) were infected by the hemlock woolly adelgid (HWA; *Adelges tsugae*) in 2009 after initial detection at the site in 2008, and selected for long-term monitoring due to their contrasting responses to infection. A set of six automated soil respiration chambers were established in each stand in the mid 2010s and have since been continuously monitoring soil CO_2 flux. Within each stand, six units of Fluxbot 2.0 were deployed within the footprint of the established autochamber array, to allow direct comparison; two additional units of Fluxbot 2.0 were deployed at each (eight total per stand) as backups to ensure data continuity.

2.1. Site/context description

In the fall of 2015, six automated soil respiration chambers were established within the footprint of the Hemlock tower (42.529162, -72.178581) at Harvard Forest LTER. The hemlock tower stand (hereafter "stand 2") has distinct hemlock loss and high stand biodiversity in overstory and understory plant communities. A second set of six chambers were established in May 2016 downstream from the Bigelow Brook weir (42.541500, -72.174624). Contrary to stand 2, this stand ("stand 1") continued to resemble an uninfected hemlock stand in hemlock loss and community composition despite infection.

2.2. Harvard Forest autochambers

The six autochambers per site are arrayed in a circle around a control box. The collars are 7cm long segments of schedule 80 PVC pipe installed approximately 3 cm into the soil; PVC diameter is approximately 11 inches. Chamber lids open and close pneumatically every 30 minutes using AC line power.

The control box at the center of each autochamber array includes the infrared gas analyzers (IRGA) and power equipment. The IRGA at the hemlock tower is a LI-840 (LI-COR Lincoln, NE, USA), and at Bigelow Brook is a LI-800 (LI-COR). The other mechanics include a pump (Brailsford TD-3LS 12VDC), a CR1000 datalogger, a SDM-CD16AC relay controller, and a 12VDC power supply. Critically, the chambers are plumbed to an array of solenoid valves also at the control box, that move compressed air to and from the pistons that open and close the chamber lids and move sampled air from the chambers to the IRGA. The chambers are activated sequentially every 5 minutes to enable measurement at each of the six chambers, every 30 minutes. Each measurement lasts for five minutes total: for the first 45 seconds, the chamber lid remains open and air is drawn at 1 liter per minute. The lid then closes and internal CO_2 concentration is recorded at 1hz rate for four minutes, 15 seconds. At the completion of each five-minute measurement cycle the chamber lid reopens.

The LI-840 at stand 2 measures CO_2 and H_2O and applies a correction for water vapor in the sample air. The LI-800 at stand 1 does not correct for water vapor automatically. A subset of historical flux measurements from the LI-800 were recalculated using the water vapor correction applied to simultaneously-collected LI-840 data. The correction underestimated the fluxes by only 0.016% ± 2%; as a result, the LI-800 data does not include a correction factor.

Photo 1 | Field deployment of soil CO_2 flux monitoring systems at Harvard Forest. The image shows both Fluxbot 2.0 and autochamber systems deployed side-by-side in a hemlock forest stand. The larger pneumatically-operated autochambers are connected via tubing to a central control box containing the infrared gas analyzer (IRGA), while the smaller autonomous Fluxbot 2.0 units operate independently with integrated CO_2 sensors and servo-actuated lids. The inset shows a close-up of a Fluxbot 2.0 unit with its hinged lid design and compact, battery-powered configuration. This co-located deployment enabled direct comparison of flux measurements between the two systems under identical field conditions.

2.3. Fluxbot array

Eight Fluxbot 2.0 chambers were deployed at each of the two sites at Harvard Forest. Six Fluxbots were paired with autochambers to enable direct comparisons of flux measurements, while two additional units were deployed as backups to ensure continuity in case of system failure, such that eight fluxbots were distributed approximately evenly throughout the plot. Fluxbots were installed on 4-inch SCH 40 PVC collars inserted approximately 4 cm into the soil. The chambers, constructed from commercially available PVC sewer caps with hinged lids, were actuated by servo motors on a 60-minute cycle. During each cycle, the lids closed to create an

airtight environment for soil CO_2 flux measurements and reopened to restore ambient conditions between measurements. Fluxbots were positioned within each site to capture local heterogeneity in microtopography and vegetation. This distributed configuration ensured that flux variability across the array was representative of site-scale conditions.

Each Fluxbot was equipped with a Senseair K30 nondispersive infrared (NDIR) CO_2 sensor inside the chamber lid, which measured CO_2 accumulation within the closed chamber diffusively (i.e., not plumbed from the exterior to the interior with tubing and a fan). The K30 has a detection range of 0–10,000 ppm; for each measurement period at the end of each hour, they were set to record at a frequency of 1Hz for six minutes total (one minute while chamber is open to capture ambient CO_2 concentration; five minutes while chamber is closed to capture accumulation). Environmental conditions were monitored with a Sensirion SHT-30 (air temperature and relative humidity) and an LPS22 (barometric pressure), both deployed adjacent to the K30 inside the chamber lid. Each Fluxbot was powered by a Voltaic Systems V50 battery pack, which provided up to 13 days of continuous operation before needing recharging. Data collection, sensor operation, and lid actuation were managed by a Particle Boron microcontroller, which also transmitted measurements hourly via LTE cellular networks to a Google Sheet document. The modular, independently-operating, and weatherproofed design (including PTFE envelopes around the K30 sensor to prevent condensation, and reflective shields over the SHT to prevent errors in temperature detection from direct sunlight). A full description of system engineering and performance metrics is provided in (Pan et al. 2024).

The updated Fluxbot 2.0 boasts several improvements from the original design (Forbes et al. 2023). Battery life is extended from ~24hrs to >300hrs, and wireless data transmission capabilities allows for user monitoring from remote locations. Fluxbot 2.0 also has improved weatherproofing and simplified assembly, but maintains the core benefits of low individual cost (~400 USD in parts), independence (i.e., not multiplexed), and mechanistic reproducibility.

2.4. Fluxbot-chamber comparison experiment

The paired Fluxbot and autochamber systems were operated concurrently at each site to evaluate the performance of the Fluxbot system relative to the established autochambers under identical environmental conditions. Flux measurements from both systems were calculated from raw data, using the same standardized processing methods to ensure consistency. These comparisons were analyzed to assess whether Fluxbots could replicate the mean fluxes, temporal trends, and spatial variability observed with autochambers, addressing the study's broader goal of evaluating the scalability and ecological applicability of the Fluxbot system across diverse forest conditions.

2.5. Additional environmental data

Air pressure and soil temperature data used in this study were obtained from the Fisher Meteorological Station at Harvard Forest (Harvard Forest Data Archive: HF001). The station, located at 42.53311°N, -72.18968°W, is approximately 1.55 km from stand 1 (Bigelow Brook

Weir) and 1.01 km from stand 2 (Hemlock Tower). Air pressure was measured using a Vaisala CS105 barometer, and soil temperature at 10 cm depth was recorded using Campbell Scientific 107 probes. For this study, we used average hourly values to align with the temporal resolution of fluxbot measurements. These data are publicly available as part of the Harvard Forest LTER) program and are accessible via the Environmental Data Initiative (Boose and VanScoy 2025).

2.6. Data processing and calculation

Raw data (e.g., times series of CO_2 concentrations for each observation interval) was converted to flux for each array in the following manner. One minute of raw concentration data is trimmed from the start of the five-minute chamber closure period to account for the "dead band", or period of time during and after chamber closure during which the interior volume is not yet thoroughly mixed (and detection of interior gas concentration is not yet reliable). The remaining four minutes of data are converted from ppm (concentration) to umol CO_2 (mass) using ideal gas laws, including chamber volume plus the internal volume temperature data collected from each chamber's accessory gas analyzers (Forbes et al. 2023), and atmospheric pressure data collected by the Fisher Meteorological Station (see above). Subsequently, change in CO_2 mass is determined by calculating both linear and quadratic regressions of these four minutes of data; the initial slope of each regression is then used to calculate change in CO_2 mass over the interval, over the area of the collar on which the chamber sits.

Fluxbot 2.0 array: Because the Fluxbot 2.0 has a relative humidity sensor inside the chamber, flux estimates included a humidity correction based on the density of water vapor inside the chamber volume over the course of a measurement interval. Fluxbot 2.0 chamber volume was (on average) 768cm^3; chamber area was 81cm^2.

Autochamber chamber volumes ranged from 9450cm^3 to 10450cm^3, while area for all chambers was 646.328cm^2. Because there was only a relative humidity sensor on one of the two control boxes, the flux estimates generated for the autochamber arrays were not corrected for humidity (see above).

3. Results

3.1. Temporal Trends and System Performance

During the October 2-31, 2023 deployment period, both Fluxbots and autochambers maintained high operational reliability, with data capture rates exceeding 95% despite periodic interruptions in power or data transmission. Both systems captured consistent temporal trends in soil CO_2 flux measurements. Figure 1 presents the calculated fluxes and rolling 6-day means, which interpolate across gaps caused by system downtime. Soil temperature at 10 cm depth, measured hourly, is shown alongside flux data and highlights environmental variability during the study period.

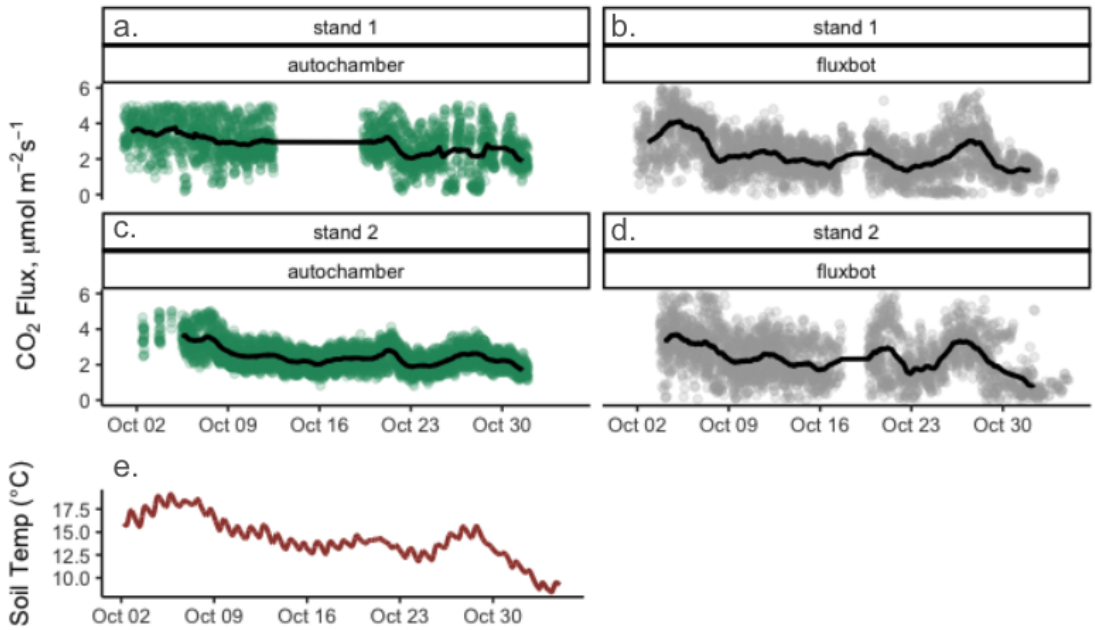

Fig. 1 | Panels a-d: Calculated fluxes and rolling mean for each array. Arrays were deployed from October 2-31, 2023 but experienced variable downtime, accounting for the data gaps seen here. Black lines are 6-day rolling means (filled with adjacent values during system downtime). **Panel e: Soil temperature from Fisher meteorological station.** Soil temperature measured hourly at 10cm depth and available through the Harvard Forest archive.

3.2. Chamber-Level Flux Distributions

Chamber-level analysis revealed consistent patterns in flux variability across both stands. Individual chamber medians ranged from approximately 1.5 to 4.0 µmol $m^{-2}s^{-1}$, with interquartile ranges spanning 0.9-4.4 µmol $m^{-2}s^{-1}$. The similar spread in chamber-level distributions between methods supports the equivalence of spatial characterization between systems.

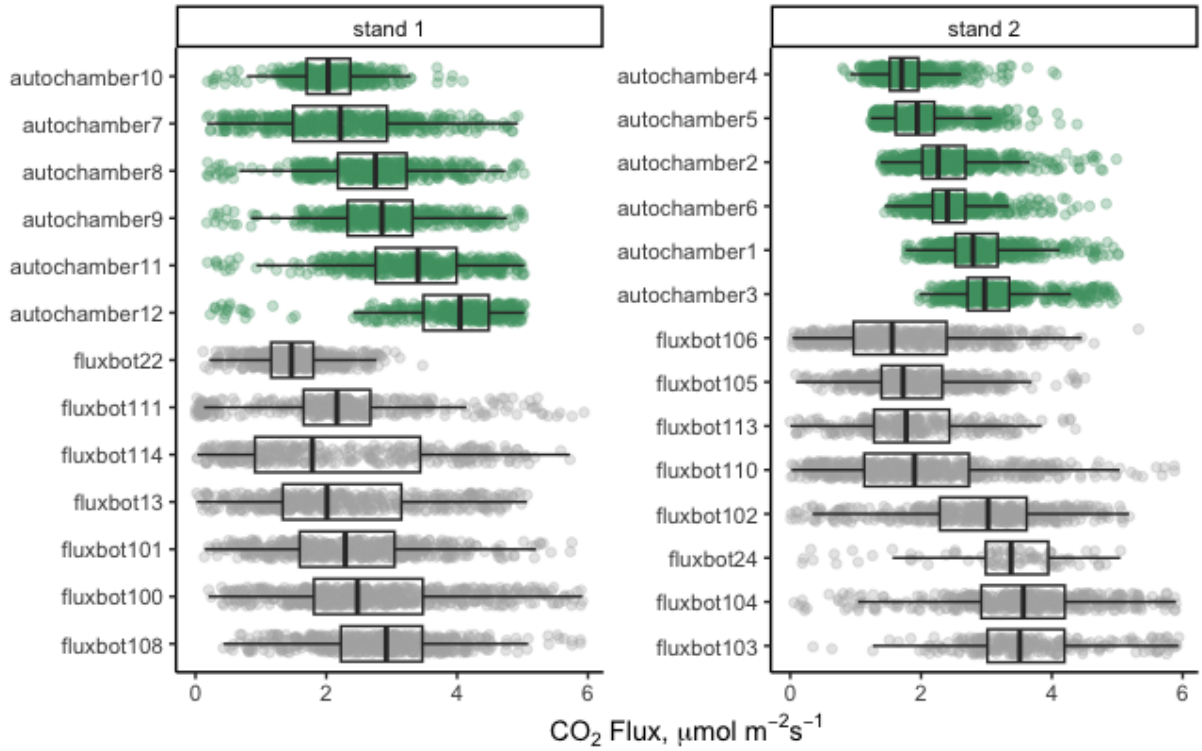

Fig. 2 | Distributions of chamber-level fluxes. Chambers are grouped by stand within separate plots for each array (fluxbots and autochambers). In each boxplot, the middle horizontal line represents the median flux value, while the upper and lower edges of the box mark the 75th and 25th percentiles, respectively (the interquartile range, IQR). The whiskers extend to the most extreme values within 1.5 times the IQR from the quartiles. Chambers are plotted in order from lowest to highest mean flux for ease of interpretation.

3.3. Statistical Validation and Model Performance

The generalized additive model (GAM) analysis (Table 1) provided robust statistical validation of the Fluxbot system, explaining 54.1% of observed variance (Figure 3). The GAM revealed no significant differences between stand 1 and stand 2 plots (β = -0.013, SE = 0.249, p = 0.958) or between arrays (β = -0.332, SE = 0.250, p = 0.185). Smoothing terms (hour of day and soil temperature) were highly significant ($p < 2e\text{-}16$), indicating strong temporal structure in the flux measurements.

Table 1 | Generalized additive model results for soil CO_2 flux measurements. The model includes fixed effects for forest stand (Stand 2 vs. Stand 1) and measurement method (Fluxbot 2.0 vs. autochamber), with smooth terms for hour of day, individual chamber identity, and soil temperature at 10 cm depth (s10t).

Parameter	Estimate/edf	Std. Error/Ref.df	t/F value	p-value
(Intercept)	2.68731	0.22411	11.991	<2e-16 ***
Stand 2	-0.01306	0.24887	-0.052	0.958
Method: fluxbot 2.0	-0.33194	0.25024	-1.326	0.185
s(hour(hour_of_obs))	6.367	7.516	15.69	<2e-16 ***
s(id)	23.926	24.000	356.24	<2e-16 ***
s(s10t)	8.180	8.735	792.91	<2e-16 ***

Model Summary: R-sq.(adj) = 0.541, Deviance explained = 54.3%, n = 13591 Significance codes: 0 **" 0.001 "** 0.01 " 0.05 '.' 0.1 ' ' 1

The GAM analysis revealed no significant differences between forest stands (p = 0.958) or measurement methods (p = 0.185), indicating that both hemlock stands exhibited similar flux patterns during the study period, and that Fluxbot 2.0 measurements were statistically equivalent to autochamber measurements. Given these findings, subsequent analyses pooled data across both stands to compare system performance (all autochambers vs. all Fluxbots).

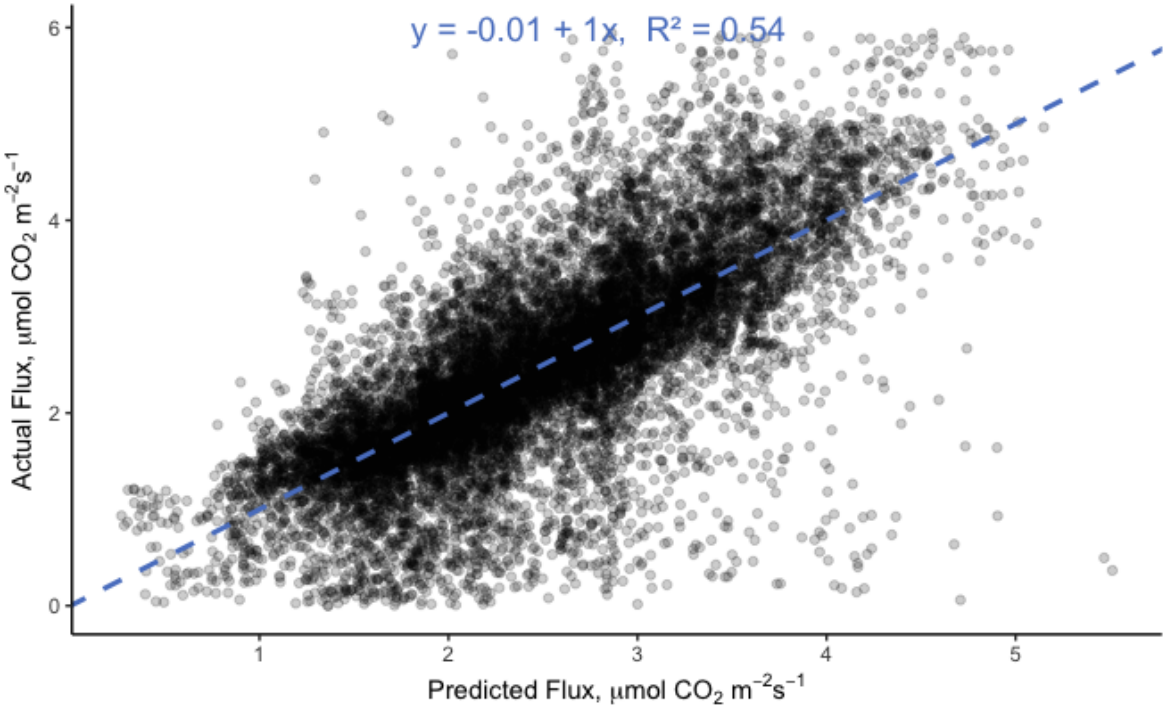

Fig. 3 | Modeled soil respiration across the entire dataset. Generalized additive model using fixed effect of stand and array method (fluxbot or autochamber); smoothed fixed effect of hour of day and day of year; and random effect of chamber ID. Scatterplot shows predicted vs. actual flux and hypothetical 1:1 line.

3.4. Measurement Distribution and System Agreement

The distribution of individual flux measurements showed strong concordance between systems (Figure 4). Both methods captured a similar range of flux values (approximately 0-6 µmol $m^{-2}s^{-1}$) with comparable central tendencies, illustrated by overlapping kernel density estimates. The slightly wider distribution in Fluxbot 2.0 measurements suggests marginally higher measurement variability, potentially due to the different sensor input employed (diffusion-based sensing within each unit, versus flow-through to a common IRGA for the autochambers), or the smaller area covered by the Fluxbot 2.0 collar footprint (4” diameter versus approximately 11” diameter of the autochamber collars).

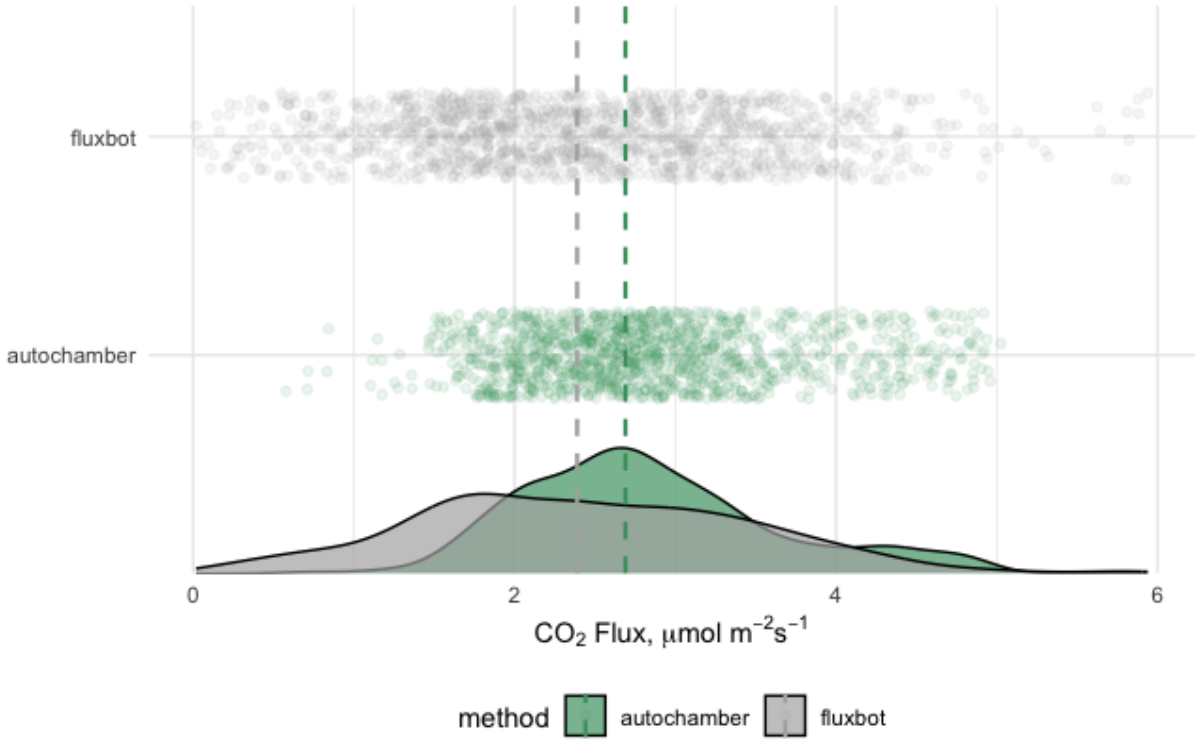

Fig. 4 |Scatterplot and density plot showing flux estimates from each array. The upper panel displays individual flux measurements from fluxbots (top) and autochambers (bottom) as jittered scatter points, with vertical dashed lines representing the mean flux for each method. The lower panel illustrates the kernel density estimates for the flux values from both methods, indicating the distribution of flux measurements. Fluxbot data are shown in grey, and autochamber data are shown in green. The vertical dashed lines indicate the respective mean flux values for each method. This visualization highlights both the distribution and central tendency of flux measurements from the two sensor systems.

Quantitative comparison of 3-hour rolling mean fluxes demonstrated strong agreement between systems (Figure 5). Lin's Concordance Correlation Coefficient (CCC) accounts for both precision and accuracy, providing a more comprehensive measure of agreement than simple correlation (R^2). Unlike regular correlation (which only measures if two datasets follow similar patterns), CCC penalizes systematic differences between methods by combining two components: how well the data points fit along any straight line (precision) and how close that line is to the perfect 1:1 diagonal where both methods give identical readings (accuracy); CCC value close to 1 indicates strong agreement between the systems (Akoglu 2018; Lin 1989). The 3-hour rolling mean demonstrated CCC of 0.7 and linear regression parameters of $y = -0.49 + 1.09x$ ($R^2 = 0.67$). The regression slope of 1.09 indicates minimal proportional bias, while the small intercept (-0.49) suggests negligible systematic offset between methods. The moderate R^2 value reflects natural variability in soil flux measurements rather than methodological disagreement, as evidenced by the tight confidence intervals around the regression line.

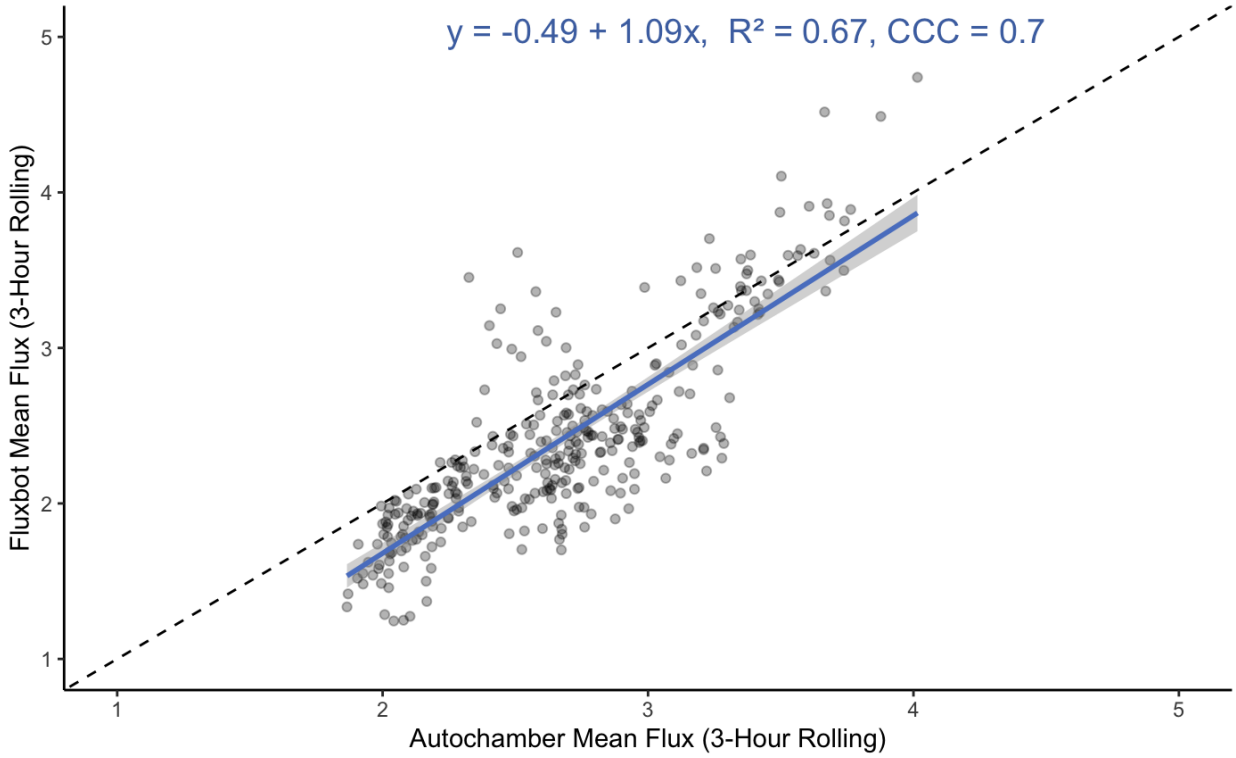

Fig. 5 | Agreement between array-wide mean fluxes. Scatterplot showing 3-hour rolling means of flux estimates from fluxbots and autochambers. Each point represents the paired rolling mean of flux measurements between the two sensor systems at the corresponding time intervals. The x-axis represents the 3-hour rolling mean flux from the fluxbots, while the y-axis represents the 3-hour rolling mean flux from the autochambers. The plot highlights the relationship and agreement between the two measurement systems across the observation period. The degree of agreement between the systems is quantified using Lin's Concordance Correlation Coefficient (CCC).

3.5. Diurnal Patterns and Temporal Dynamics

Both systems captured pronounced diurnal patterns in soil CO_2 flux (Figure 6), with remarkable consistency in the timing and magnitude of daily cycles. Peak fluxes occurred during midday hours (approximately 15:00-17:00 local time), reaching mean values of 2.7 ± 0.1 μmol $m^{-2}s^{-1}$, while minimum fluxes were observed in early morning hours (04:00-06:00) at around 2.3 ± 0.1 μmol $m^{-2}s^{-1}$. The 95% confidence intervals remained consistently narrow (±0.1-0.2 μmol $m^{-2}s^{-1}$) throughout the daily cycle for both systems, indicating high measurement precision and reproducibility.

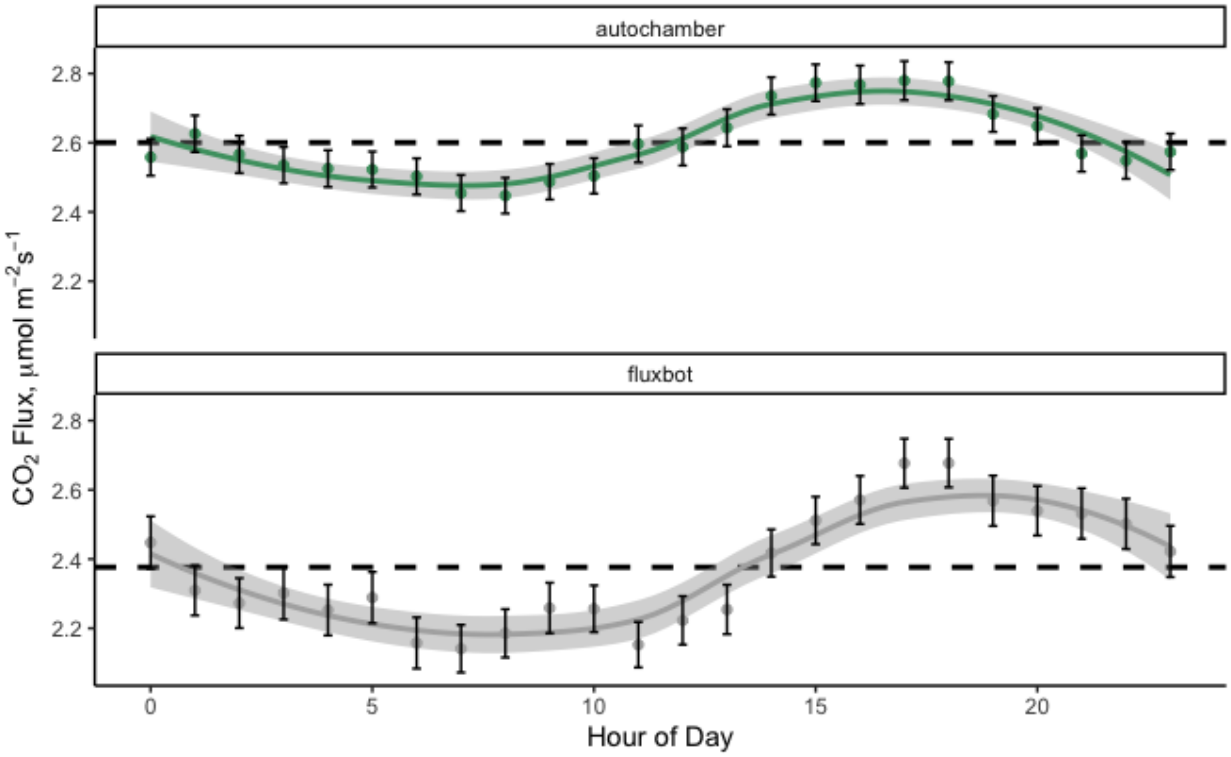

Fig. 6 | Diurnal variation in flux estimates measured by autochambers (top panel) and fluxbots (bottom panel) over the course of the day. The smooth lines represent the fitted trends with 95% confidence intervals (shaded areas) for each method, showing the diurnal pattern of fluxes. Points correspond to the hourly mean flux estimates, with error bars representing the standard error of the mean. The dashed black horizontal lines indicate the overall mean flux for each method.

3.6. Temperature Response

Temperature sensitivity analysis revealed comparable Q10 values (a standardized measure of how soil respiration rates respond to temperature changes, calculated as the factor by which CO_2 emissions increase per 10°C warming) between systems (Figure 7). Autochambers exhibited a Q10 of 2.31 across an observed temperature range of 11.2-19.1°C, while Fluxbots showed a Q10 of 2.86 across an observed temperature range of 8.5-19.1°C. The observed values of 2.31-2.86 indicate that soil microbial and root activity roughly doubles to triples with each 10°C temperature rise ; these values fall within a typical range for temperate forest soils. Exponential temperature-flux relationships showed moderate explanatory power (R^2 = 0.25 and 0.22 for autochambers and fluxbots, respectively), reflecting the natural variability inherent in soil respiration processes.

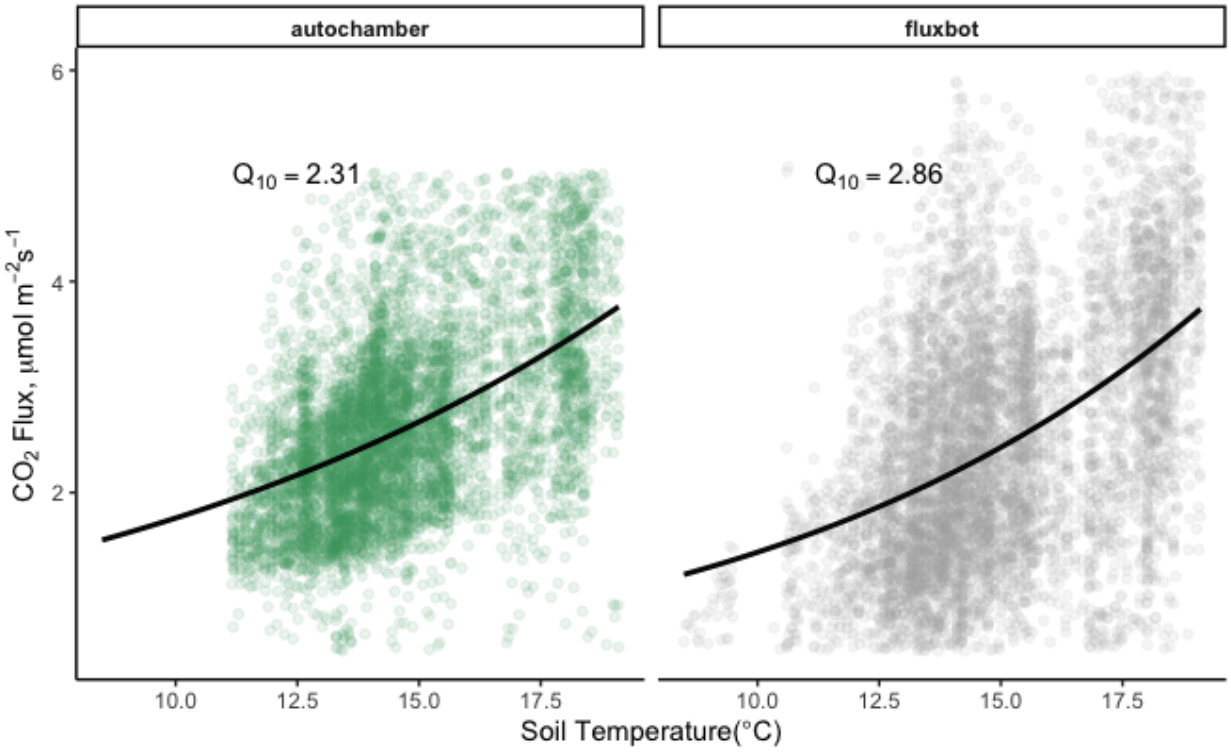

Fig. 7 | Scatterplot showing the Q10 models for soil respiration flux for Autochambers (green) and Fluxbots (grey). Solid line represents the fitted Q10 model for autochambers, and the dashed line represents the fitted Q10 model for fluxbots. Points indicate individual flux measurements.

3.7. Spatial Heterogeneity

Analysis of spatial variability using Lorenz curves revealed identical Gini coefficients of 0.13 for autochamber array, and only marginally more variable (0.16) for the Fluxbot 2.0 array (Figure 8), indicating almost consistent characterization of flux heterogeneity. Lorenz curves graphically visualize spatial distribution by plotting cumulative percentage of a value (here, total flux) against cumulative percentage of observations (here, measurement locations) ranked from lowest to highest contribution, with deviation from the diagonal line of perfect equality indicating spatial inequality. The Gini coefficient quantifies this inequality, ranging from 0 (perfectly uniform distribution) to 1 (maximum concentration in few locations). The relatively low Gini coefficient here suggests moderate spatial homogeneity in flux patterns, with approximately 60% of total measured flux coming from 50% of sampling locations. The relative agreement in Gini coefficients between methods provides strong evidence that Fluxbot 2.0 can effectively replicate the spatial resolution capabilities of traditional autochambers, and the slight difference in agreement is likely reflective of the smaller footprint of Fluxbot 2.0 compared to an autochamber, as smaller measurement areas are more likely to capture localized variability that larger areas would average out.

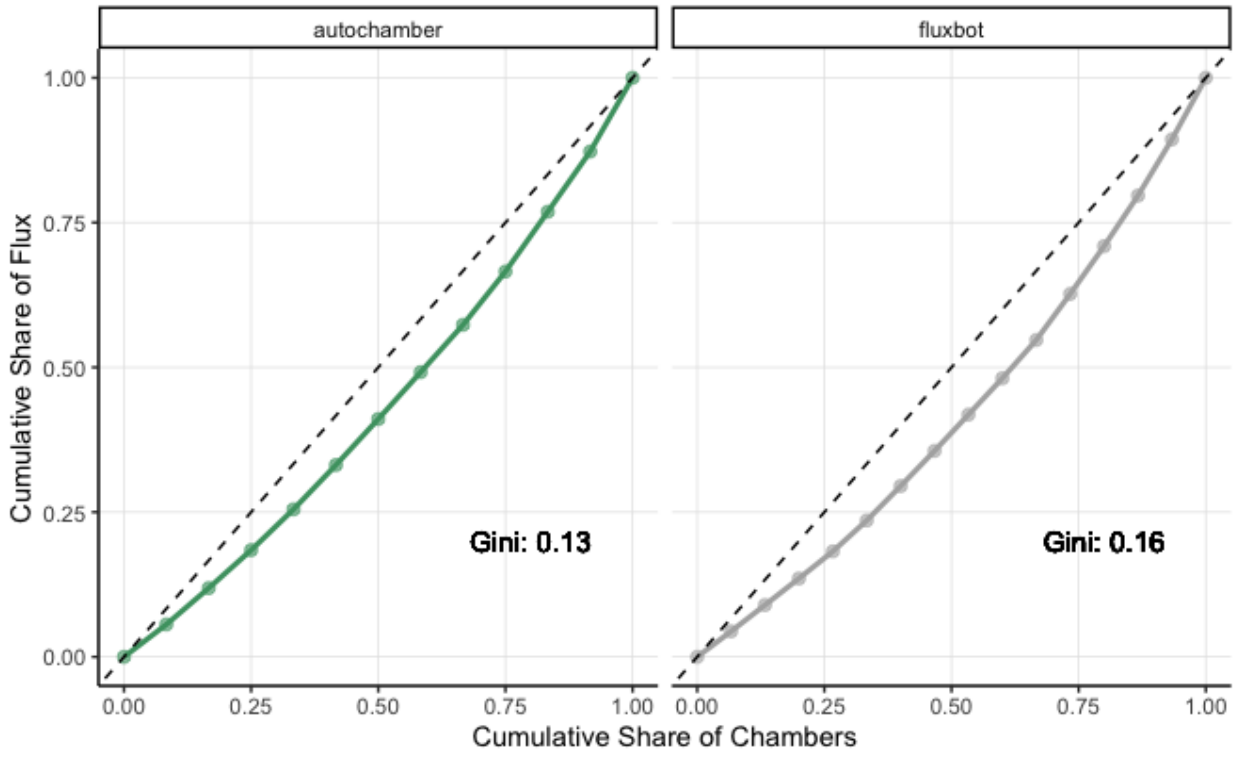

Fig. 8 | Lorenz curves for each array. Lorenz curves comparing flux inequality between two measurement methods (autochamber and fluxbot). The x-axis represents the cumulative share of sensors, and the y-axis represents the cumulative share of flux. The dashed diagonal line represents perfect equality, where each sensor contributes equally to the total flux. The deviation of each Lorenz curve from the diagonal line indicates the degree of inequality in flux distribution. The Gini coefficient, displayed on each plot, quantifies this inequality, with values closer to 1 indicating greater inequality.

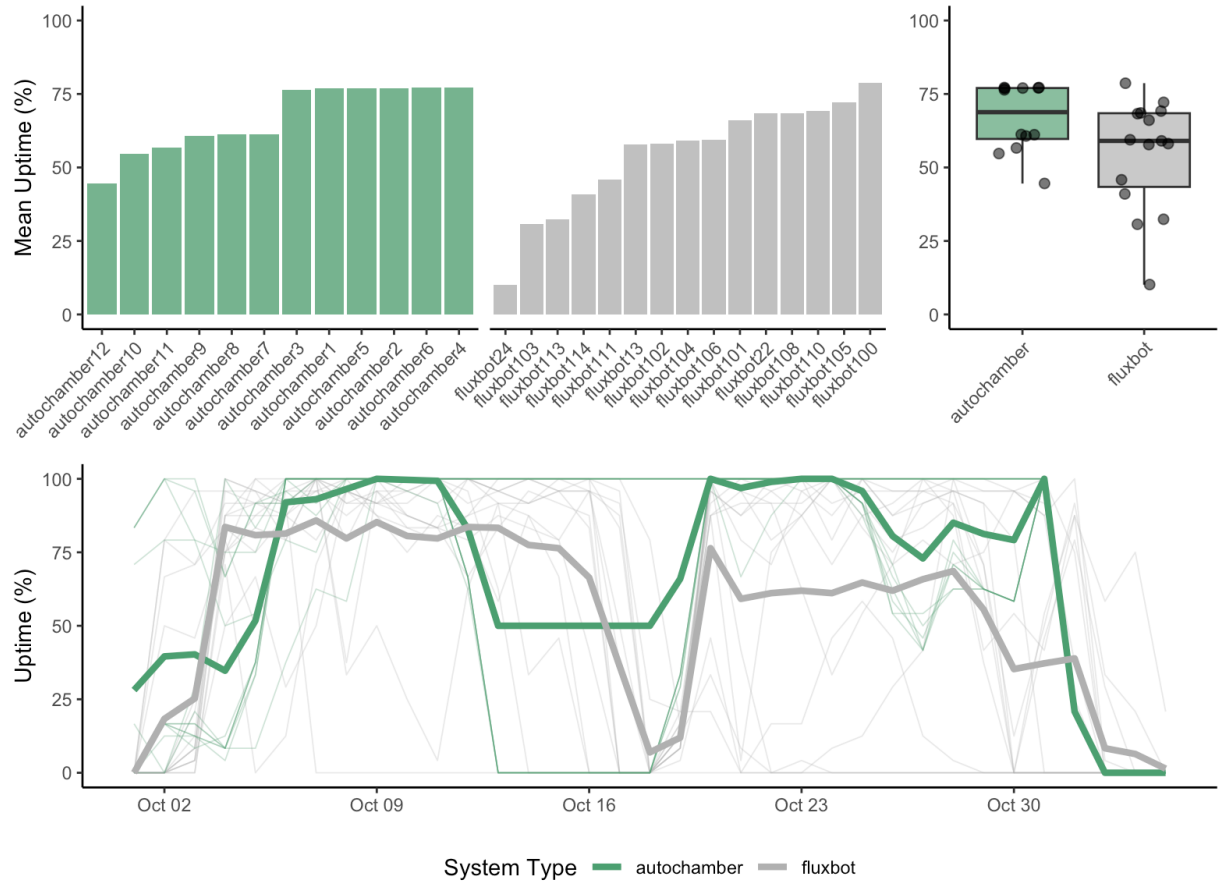

Fig. 9 | System uptime summary for autochamber and Fluxbot 2.0 arrays. Top panels: mean daily uptime for each unit (barplot, left) and distribution of mean uptime across units (boxplot, right) during the October 2023 deployment. Bottom panel: daily uptime time series, with thin lines showing individual unit performance and thick lines showing array-wide daily means. Both systems maintained high data retention (>95%) and captured consistent temporal patterns, with Fluxbot arrays demonstrating resilience to localized failures and autochambers achieving slightly higher overall data capture efficiency.

4. Discussion

4.1 System Performance and Measurement Validation

Our findings support the emerging literature that low-cost sensors provide a robust and cost-effective alternative to traditional autochamber systems for monitoring soil respiration (Harmon et al. 2015; Bastviken et al. 2015; Forbes et al. 2023). The high operational reliability (>95% uptime) and strong statistical agreement with autochambers (CCC = 0.70; Fig. 5) suggest that Fluxbot 2.0 can effectively replicate the measurement quality of established systems while offering substantial advantages in terms of deployment flexibility and cost-effectiveness

(Macagga et al. 2024; Al Hamwi et al. 2024). The precision of the Fluxbot sensors was sufficient to provide accurate flux estimates without the need for calibration to exact ("absolute") gas concentration values. This is because the flux calculation depends on the rate of change in concentration over time, not on the absolute concentration level itself (see SI). In other words, even if the sensors have a small bias in their absolute readings, the slope of the concentration increase inside the closed chamber—on which flux estimates are based—remains reliable (SI Fig. S1-S5; SI Table S1-S3). The closed-chamber accumulation approach utilized by Fluxbots has been shown to maintain robust performance without frequent calibration (Brecheisen et al. 2019; Harmon et al. 2015).

From October 2-31, 2023, the Fluxbot array collected 6,824 flux measurements from 10,800 potential measurement intervals (63.2% collection rate), with 6,667 measurements retained after quality control (97.7% retention rate), yielding an overall success rate of 61.7%. The autochamber array collected 13,525 flux measurements from 17,280 potential measurements (78.3% collection rate), with 12,926 measurements retained after quality control (95.6% retention rate), yielding an overall success rate of 74.8%. Both systems demonstrated excellent data quality with retention rates exceeding 95%. This comprehensive dataset demonstrates the scalability of automated chamber approaches (Liang et al. 2003) while maintaining measurement quality across distributed arrays.

While the autochamber system achieved higher overall data collection efficiency, the system was more vulnerable to periods of complete shutdown. Because fluxbots are autonomous, the fluxbot array remained more resilient than the autochamber array; during times of lost power or pneumatic malfunctions, the entire autochamber array in a given location would fail, resulting in longer periods with no data collected whatsoever (Fig. 9; SI Fig. 6) . System reliability over the 30-day deployment period revealed that the Fluxbot array maintained replicated plot-level coverage (defined as ≥3 units collecting data per plot per observation interval) 90.7% of the time in stand 1 and 80.4% of the time in stand 2; while autochambers maintained coverage only 70.6% of the time in stand 1, and 89.3% of the time in stand 2. Thus, the system offers trade-offs but some benefits for ensuring reliability in a distributed array, which could be beneficial particularly for monitoring efforts focused on comparing plots in different landscapes or treatment conditions.

The moderate R^2 value (0.67) in direct comparisons between rolling average estimates of fluxes between the fluxbot and autochamber arrays reflects the complex nature of soil CO_2 flux measurements. While perfect 1:1 correlation at fine temporal and spatial scales is not expected, emergent patterns in overall distributions (Figure 4) and at plot-level scales and in temporal responses show strong concordance between measurement systems. Microbial and root processes that drive soil respiration are both spatially and temporally dynamic, with multiple drivers regulating instantaneous flux at any given moment (Bradford and Ryan 2008; Vargas et al.

2011). This inherent variability manifests across scales, from sub-meter heterogeneity to landscape patterns (Martin and Bolstad 2009).

4.2 Temporal Resolution and Environmental Response

The clear and consistent diurnal patterns captured by both systems demonstrate the Fluxbots' capability to resolve fine-scale temporal dynamics in soil respiration. Both systems detected consistent diel flux patterns (Fig. 6), with peak activity during midday hours reflecting the integration of temperature-dependent root respiration, microbial activity, and potential lagged responses to photosynthetic carbon allocation (Savage & Davidson, 2003; Tang et al., 2005) (Table 2). These temporal patterns tracked well with soil temperature (Figure 1), demonstrating the importance of environmental drivers in shaping flux dynamics (Hollinger et al., 2004).

Table 2 | Summary statistics of soil CO_2 flux measurements during peak and minimum daily periods. Mean, median, 95th percentile, and standard error values for Fluxbot 2.0 and autochamber arrays during evening hours (15:00-20:00) and morning hours (05:00-10:00), corresponding to periods of maximum and minimum daily flux, respectively. Data are stratified by measurement system, time period, and forest stand to illustrate diurnal patterns and system performance across different site conditions during the October 2023 deployment period.

Summary Statistics: Flux by Array type, Location, and Approx. Min/Max Time of Day

			Summary Statistics				
Array	**Stand**	**Time of day**	**Mean**	**Median**	**95th Percentile**	**SE**	**N**
Autochamber array:							
autochamber	stand 1	evening	3.03	2.97	4.61	0.05	325
autochamber	stand 1	morning	2.81	2.77	4.60	0.05	368
autochamber	stand 2	evening	2.60	2.58	4.12	0.03	502
autochamber	stand 2	morning	2.30	2.22	3.36	0.03	468
Fluxbot array:							
fluxbot	stand 1	evening	2.66	2.56	4.68	0.05	458
fluxbot	stand 1	morning	2.27	2.04	4.41	0.05	409
fluxbot	stand 2	evening	2.70	2.60	4.65	0.06	407
fluxbot	stand 2	morning	2.39	2.26	4.49	0.06	389

Note:
SE = Standard Error
P95 = 95th Percentile
N = number of flux obs.
morning = 5am - 10am
evening = 3pm - 8pm

The temperature sensitivity of respiration, calculated as Q10, is a critical parameter in understanding soil carbon dynamics. Our observed Q10 values (2.31 for autochambers and 2.86 for Fluxbot 2.0; Figure 7) fall within the range commonly reported in the literature for temperate forest soils (typically 2.0 to 3.0) (Davidson and Janssens 2006). The slightly higher Q10 value for Fluxbot 2.0 might reflect differences in chamber design affecting soil microclimate or variations in sensor response characteristics: specifically, a significantly smaller collar footprint resulting in a significantly smaller area measured. Seminal studies (Lloyd and Taylor 1994) have shown that Q10 values can vary significantly depending on soil type, moisture, and biological activity, reinforcing the importance of continuous, high-resolution measurements. Critically, both systems captured broader temporal trends, such as seasonal shifts in flux patterns. The ability to detect such trends is essential for understanding long-term ecosystem carbon dynamics and responses to environmental change (Jian et al. 2018).

4.3 Capturing Landscape Heterogeneity

Our GAM model found no significant differences in fluxes between the hemlock stands during our October deployment. While previous work at these sites has documented differences during peak growing season, the magnitude of these differences typically dissipates during shoulder seasons as both plant and microbial processes slow (Giasson et al. 2013; Phillips et al.). The lack of between-stand differences in our study period does not diminish the demonstrated capability of the Fluxbot 2.0 arrays to accurately reproduce site means and variability across distributed patches of a landscape, especially given the similar patterns captured by the autochamber array—rather, it reflects the seasonal context of our deployment.

One of the key strengths of the Fluxbot 2.0 system is its ability to capture spatial variability in soil respiration across multiple scales. At the local scale, Fluxbots captured heterogeneity driven by microtopography, soil composition, and vegetation patterns, as evidenced by the range of individual chamber medians spanning 1.5 to 4.0 μmol $m^{-2}s^{-1}$ (Figure 2). At the landscape scale, they successfully monitored broader patterns associated with forest stand conditions and environmental gradients, demonstrating equivalent performance to autochambers in characterizing site-level flux distributions. This capability provides both mechanistic insight into localized flux drivers and a broader perspective on regional carbon budgets (Rodeghiero and Cescatti 2008). The ability to capture multiscale variability is essential for accurate ecosystem carbon accounting and for understanding the spatial distribution of soil carbon flux hotspots. The Lorenz curve analysis (Figure 8), showing very similar Gini coefficients (0.13 for autochambers and 0.16 for Fluxbot 2.0 arrays), underscores the system's effectiveness in capturing flux heterogeneity with minimal deviation from established methods.

4.4 Improving carbon cycling estimates

Other methods that currently capture high spatial coverage and resolution of soil C fluxes include tower networks, satellites, and airborne eddy covariance systems. However, these approaches

often lack the fine spatial resolution provided by distributed ground-based systems like Fluxbots. For example, eddy covariance towers provide high temporal resolution but are limited in spatial specificity, while satellite-based methods offer broad coverage but lower temporal and spatial resolution (Baldocchi 2003). Airborne eddy covariance systems can bridge some gaps but are logistically complex and costly. The concept of distributed sensor networks is not new and has been successfully applied in other fields, such as air quality monitoring for environmental and public health (Castell et al. 2017; Hasenfratz et al. 2015; Dubey et al. 2024). Low-cost air quality sensor networks have revolutionized the ability to track pollutants across urban areas, providing actionable data for policymakers and communities. Similarly, distributed Fluxbot arrays have the potential to democratize soil carbon monitoring, enabling broader participation and more comprehensive datasets for climate research.

The scalable deployment capabilities of Fluxbot 2.0 arrays extend beyond traditional carbon accounting to support emerging research areas and practical applications. In zoogeochemistry, distributed sensor networks can quantify how animal activities—from soil-dwelling invertebrates to large herbivores—create spatial patterns in biogeochemical cycling, enabling researchers to map animal-mediated carbon hotspots across landscapes. Agricultural monitoring, measurement, reporting, and verification (MMRV) protocols increasingly require high-resolution soil carbon data to validate carbon sequestration claims in regenerative farming and carbon crediting; Fluxbot 2.0 arrays can provide the temporal and spatial resolution needed to capture agricultural soil carbon dynamics, particularly in highly heterogeneous landscapes, during and after extreme weather events, and over the course of growing and non-growing seasons (Burba 2025; Bradford et al. 2025). Additionally, these systems offer valuable applications in ecosystem restoration monitoring, where tracking soil respiration recovery can indicate restoration success, and in urban ecology, where understanding soil carbon dynamics in fragmented green spaces supports sustainable city planning. The autonomous design also makes Fluxbot arrays particularly suitable for monitoring remote or inaccessible ecosystems, filling critical data gaps in global carbon cycle research and supporting evidence-based environmental management decisions across diverse landscapes.

Our results demonstrate that distributed arrays of low-cost flux chambers can effectively monitor soil carbon dynamics across heterogeneous landscapes. The validated performance of distributed Fluxbot arrays has important implications for expanding carbon monitoring beyond intensively studied research sites. The relatively low cost and simplified deployment requirements make it feasible to establish monitoring networks across larger spatial extents and in previously understudied ecosystems, similar to how other low-cost sensor networks have democratized environmental monitoring (Harmon et al. 2015; Rundel et al. 2009; Bastviken et al. 2015).

The high temporal resolution of the measurements combined with extensive spatial coverage enables detection of both fine-scale patterns and broader ecosystem-level trends (Bastviken et al. 2022). This capability opens new opportunities for studying soil carbon cycling across

landscapes and improving geographical coverage of flux measurements (Jian et al. 2018). The demonstrated ability of Fluxbots to capture both fine-scale temporal patterns and spatial heterogeneity makes them particularly valuable for studies of ecosystem response to environmental change and for improving carbon accounting in managed systems, including nature-based climate solutions where comprehensive monitoring across diverse landscapes is essential (Novick et al. 2022).

4.5 Limitations and Future Directions

While our study demonstrates the utility of Fluxbots for monitoring soil respiration, future research should focus on long-term deployments across diverse ecosystems to further validate their performance under varying environmental conditions. Additionally, integrating Fluxbot data with other remote sensing and modeling approaches could provide more comprehensive insights into soil carbon dynamics at regional and global scales.

Exploring the potential of Fluxbots for measuring other greenhouse gases (e.g., CH_4, N_2O) and incorporating additional environmental sensors could further enhance their utility in ecosystem monitoring. Addressing challenges related to sensor calibration, data transmission, and long-term maintenance will also be critical for ensuring the sustained operation of distributed sensor networks.

4.6 Conclusions

This study demonstrates that arrays of low-cost, autonomous flux chambers can effectively monitor soil carbon dynamics at both fine spatial scales and across broader landscape extents. The strong agreement between Fluxbot and autochamber measurements validates this approach for capturing spatial and temporal patterns in soil respiration. The scalability and affordability of Fluxbots open new possibilities for studying soil carbon dynamics across spatial and temporal scales previously difficult to address. By enabling expanded deployment of flux monitoring networks (Pan et al. 2024; Bastviken et al. 2015), this technology can help advance our understanding of how ecosystem structure and function influence carbon cycling across heterogeneous landscapes. Ultimately, these systems can contribute to improving ecosystem model parameterization, global carbon monitoring efforts, and our understanding of ecosystem responses to environmental change.

Acknowledgements:

We thank Connor Pan for system design and engineering leadership. Marc-Andre Giasson and Kathleen Savage contributed to establishing the autochamber systems. Xavier Murrell, Hector Castillo, Quentin Bateux, Brandon Lin, Ian Richardson, and Annise Dobson contributed to Fluxbot construction and assembly. Mark Van Scoy managed field operations and maintenance of the autochamber systems. Dave Orwig, Alassane Sow, Ravish Dubey, and Xuhui Lee provided essential context from prior research and ongoing monitoring efforts at Harvard Forest. Jackie Matthes and Peter Raymond offered valuable logistical support and insightful discussions throughout the project. We acknowledge the Harvard Forest LTER program, Emery Boose for providing meteorological data from the Fisher Meteorological Station (HF001), and Harvard Forest staff for facilitating site access and field support. This research was conducted at the Harvard Forest Long Term Ecological Research site, which is supported by the National Science Foundation LTER grant DEB-1832210.

References

1. Akoglu, Haldun. 2018. “User’s Guide to Correlation Coefficients.” *Turkish Journal of Emergency Medicine* 18 (3): 91–93.
2. Al Hamwi, Wael, Maren Dubbert, Jörg Schaller, Matthias Lück, Marten Schmidt, and Mathias Hoffmann. 2024. “Technical Note: A Low-Cost, Automatic Soil–Plant–Atmosphere Enclosure System to Investigate CO_2 and Evapotranspiration Flux Dynamics.” *Biogeosciences* 21 (24): 5639–51.
3. Baldocchi, Dennis D. 2003. “Assessing the Eddy Covariance Technique for Evaluating Carbon Dioxide Exchange Rates of Ecosystems: Past, Present and Future: CARBON BALANCE and EDDY COVARIANCE.” *Global Change Biology* 9 (4): 479–92.
4. Bastviken, D., I. Sundgren, S. Natchimuthu, H. Reyier, and M. Gålfalk. 2015. “Cost-Efficient Approaches to Measure Carbon Dioxide (CO 2) Fluxes and Concentrations in Terrestrial and Aquatic Environments Using Mini Loggers.” *Biogeosciences* 12 (12): 3849–59.
5. Bastviken, David, Julie Wilk, Nguyen Thanh Duc, Magnus Gålfalk, Martin Karlson, Tina-Simone Neset, Tomasz Opach, Alex Enrich-Prast, and Ingrid Sundgren. 2022. “Critical Method Needs in Measuring Greenhouse Gas Fluxes.” *Environmental Research Letters*, September. https://doi.org/10.1088/1748-9326/ac8fa9.
6. Bond-Lamberty, Ben, and Allison Thomson. 2010. “Temperature-Associated Increases in the Global Soil Respiration Record.” *Nature* 464 (7288): 579–82.
7. Boose, Emery, and Mark VanScoy. 2025. “Fisher Meteorological Station at Harvard Forest since 2001.” Environmental Data Initiative. https://doi.org/10.6073/PASTA/7A7FFD2EAA2EA9965D701998D4E2B1F5.
8. Bradford, John B., and Michael G. Ryan. 2008. “Quantifying Soil Respiration at Landscape Scales.” In *Field Measurements for Forest Carbon Monitoring*, 143–62. Dordrecht: Springer Netherlands.
9. Bradford, M. A., E. E. Oldfield, M. G. Arredondo, H. I. J. Black, E. S. Forbes, F. V. Jevon, C. Kelly, et al. 2025. “Agricultural Soil Carbon: A Call for Improved Evidence of Climate Mitigation.” Yale Applied Science Synthesis Program and Environmental Defense Fund white paper.
10. Brecheisen, Zachary S., Charles W. Cook, Paul R. Heine, Junmo Ryang, and Daniel Deb Richter. 2019. “Development and Deployment of a Field-Portable Soil O2 and CO2 Gas Analyzer and Sampler.” *PloS One* 14 (8): e0220176.
11. Burba, George. 2025. “Harvesting Carbon: Fields & Grasslands A Guide to Utilizing Direct Flux Measurements for Assessment and Verification of Carbon Sequestration and GHG Emission Rates over Areas.” *ESS Open Archive*. https://doi.org/10.22541/essoar.173884298.81896551/v1.
12. Carey, Joanna C., Jianwu Tang, Pamela H. Templer, Kevin D. Kroeger, Thomas W. Crowther, Andrew J. Burton, Jeffrey S. Dukes, et al. 2016. “Temperature Response of

Soil Respiration Largely Unaltered with Experimental Warming." *Proceedings of the National Academy of Sciences of the United States of America* 113 (48): 13797–802.
13. Castell, Nuria, Franck R. Dauge, Philipp Schneider, Matthias Vogt, Uri Lerner, Barak Fishbain, David Broday, and Alena Bartonova. 2017. "Can Commercial Low-Cost Sensor Platforms Contribute to Air Quality Monitoring and Exposure Estimates?" *Environment International* 99 (February): 293–302.
14. Davidson, E. A., A. D. Richardson, K. E. Savage, and D. Y. Hollinger. 2006. "A Distinct Seasonal Pattern of the Ratio of Soil Respiration to Total Ecosystem Respiration in a Spruce-dominated Forest: SEASONAL PATTERN OF THE RATIO OF SOIL-TO-ECOSYSTEM RESPIRATION." *Global Change Biology* 12 (2): 230–39.
15. Davidson, Eric A., and Ivan A. Janssens. 2006. "Temperature Sensitivity of Soil Carbon Decomposition and Feedbacks to Climate Change." *Nature* 440 (7081): 165–73.
16. DeCarlo, Keita F., and Kelly K. Caylor. 2019. "Biophysical Effects on Soil Crack Morphology in a Faunally Active Dryland Vertisol." *Geoderma* 334 (January): 134–45.
17. Dubey, Ravish, A. Telles, J. Nikkel, Chang Cao, Jonathan Gewirtzman, P. Raymond, and Xuhui Lee. 2024. "Low-Cost CO2 NDIR Sensors: Performance Evaluation and Calibration Using Machine Learning Techniques." *Sensors (Basel, Switzerland)* 24 (August). https://doi.org/10.3390/s24175675.
18. Ferraro, Kristy M., and Janey R. Lienau. 2025. "Of All Shapes and Sizes: A Theoretical Framework for Animal-mediated Terrestrial Heterogeneity across Scales." *Ecography*, no. e08006 (May). https://doi.org/10.1002/ecog.08006.
19. Forbes, Elizabeth, Vincent Benenati, Spencer Frey, Mare Hirsch, George Koech, Grace Lewin, John Naisikie Mantas, and Kelly Caylor. 2023. "Fluxbots: A Method for Building, Deploying, Collecting and Analyzing Data from an Array of Inexpensive, Autonomous Soil Carbon Flux Chambers." *Journal of Geophysical Research. Biogeosciences* 128 (6): e2023JG007451.
20. Forbes, Elizabeth S., J. Hall Cushman, Deron E. Burkepile, Truman P. Young, Maggie Klope, and Hillary S. Young. 2019. "Synthesizing the Effects of Large, Wild Herbivore Exclusion on Ecosystem Function." *Functional Ecology* 33 (9): 1597–1610.
21. Friedlingstein, Pierre, Michael O'Sullivan, Matthew W. Jones, Robbie M. Andrew, Judith Hauck, Peter Landschützer, Corinne Le Quéré, et al. 2025. "Global Carbon Budget 2024." *Earth System Science Data* 17 (3): 965–1039.
22. Gachibu, Wangari E., Mwanake R. Mwangada, T. Houska, D. Kraus, G. M. Gettel, R. Kiese, and Butterbach-Bahl. 2023. "Identifying Landscape Hot and Cold Spots of Soil Greenhouse Gas Fluxes by Combining Field Measurements and Remote Sensing Data." *Biogeosciences* 20 (24): 5029–67.
23. Garvey, Sarah M., Pamela H. Templer, Erin A. Pierce, Andrew B. Reinmann, and Lucy R. Hutyra. 2022. "Diverging Patterns at the Forest Edge: Soil Respiration Dynamics of Fragmented Forests in Urban and Rural Areas." *Global Change Biology* 28 (9): 3094–3109.

24. Giasson, M-A, A. M. Ellison, R. D. Bowden, P. M. Crill, E. A. Davidson, J. E. Drake, S. D. Frey, et al. 2013. “Soil Respiration in a Northeastern US Temperate Forest: A 22-Year Synthesis.” *Ecosphere (Washington, D.C)* 4 (11): art140.
25. Harmon, Thomas C., Diego Dierick, Nicole Trahan, Michael F. Allen, Philip W. Rundel, Steven F. Oberbauer, Luitgard Schwendenmann, and Tamara J. Zelikova. 2015. “Low-cost Soil CO_2 Efflux and Point Concentration Sensing Systems for Terrestrial Ecology Applications.” *Methods in Ecology and Evolution* 6 (11): 1358–62.
26. Hasenfratz, David, Olga Saukh, Christoph Walser, Christoph Hueglin, Martin Fierz, Tabita Arn, Jan Beutel, and Lothar Thiele. 2015. “Deriving High-Resolution Urban Air Pollution Maps Using Mobile Sensor Nodes.” *Pervasive and Mobile Computing* 16 (January): 268–85.
27. Hashimoto, Shoji, Akihiko Ito, and Kazuya Nishina. 2023. “Divergent Data-Driven Estimates of Global Soil Respiration.” *Communications Earth & Environment* 4 (1): 1–8.
28. Hollinger, D. Y., J. Aber, B. Dail, E. A. Davidson, S. M. Goltz, H. Hughes, M. Y. Leclerc, et al. 2004. “Spatial and Temporal Variability in Forest–Atmosphere CO_2 Exchange: FOREST-ATMOSPHERE CO2 EXCHANGE.” *Global Change Biology* 10 (10): 1689–1706.
29. Huang, Ni, Li Wang, Xiao-Peng Song, T. Andrew Black, Rachhpal S. Jassal, Ranga B. Myneni, Chaoyang Wu, et al. 2020. “Spatial and Temporal Variations in Global Soil Respiration and Their Relationships with Climate and Land Cover.” *Science Advances* 6 (41): eabb8508.
30. Jevon, F., Jonathan Gewirtzman, A. Lang, M. P. Ayres, and J. Matthes. 2023. “Tree Species Effects on Soil CO2 and CH4 Fluxes in a Mixed Temperate Forest.” *Ecosystems* 26 (May): 1587–1602.
31. Jian, Jinshi, Meredith K. Steele, R. Quinn Thomas, Susan D. Day, and Steven C. Hodges. 2018. “Constraining Estimates of Global Soil Respiration by Quantifying Sources of Variability.” *Global Change Biology* 24 (9): 4143–59.
32. Keiser, Ashley D., Christina L. Davis, Montana Smith, Sheryl L. Bell, Erik A. Hobbie, and Kirsten S. Hofmockel. 2024. “Depth and Microtopography Influence Microbial Biogeochemical Processes in a Forested Peatland.” *Plant and Soil*, August. https://doi.org/10.1007/s11104-024-06895-1.
33. Kim, Nakian, Chunhwa Jang, Wendy H. Yang, Kaiyu Guan, Evan H. DeLucia, and Dokyoung Lee. 2025. “Spatial Variability of Agricultural Soil Carbon Dioxide and Nitrous Oxide Fluxes: Characterization and Recommendations from Spatially High-Resolution, Multi-Year Dataset.” *Agriculture, Ecosystems & Environment* 387 (109636): 109636.
34. Leon, Elievf, Rodrigo Vargas, Stephen Bullock, Eulogio Lopez, Alan Rodrigo Panosso, and Newton La Scala Jr. 2014. “Hot Spots, Hot Moments, and Spatio-Temporal Controls on Soil CO2 Efflux in a Water-Limited Ecosystem.” *Soil Biology & Biochemistry* 77 (October): 12–21.

35. Liang, N., G. Inoue, and Y. Fujinuma. 2003. “A Multichannel Automated Chamber System for Continuous Measurement of Forest Soil CO2 Efflux.” *Tree Physiology* 23 (12): 825–32.
36. Lin, L. I. 1989. “A Concordance Correlation Coefficient to Evaluate Reproducibility.” *Biometrics* 45 (1): 255–68.
37. Lloyd, J., and John A. Taylor. 1994. “On the Temperature Dependence of Soil Respiration.” *Functional Ecology* 8 (June): 315–23.
38. Macagga, Reena, Michael Asante, Geoffroy Sossa, Danica Antonijević, Maren Dubbert, and Mathias Hoffmann. 2024. “Validation and Field Application of a Low-Cost Device to Measure CO_2 and Evapotranspiration (ET) Fluxes.” *Atmospheric Measurement Techniques* 17 (4): 1317–32.
39. Martin, Jonathan G., and Paul V. Bolstad. 2009. “Variation of Soil Respiration at Three Spatial Scales: Components within Measurements, Intra-Site Variation and Patterns on the Landscape.” *Soil Biology & Biochemistry* 41 (3): 530–43.
40. Novick, Kimberly A., Stefan Metzger, William R. L. Anderegg, Mallory Barnes, Daniela S. Cala, Kaiyu Guan, Kyle S. Hemes, et al. 2022. “Informing Nature-Based Climate Solutions for the United States with the Best-Available Science.” *Global Change Biology* 28 (12): 3778–94.
41. Ohashi, Mizue, Tomonori Kume, Seiki Yamane, and Masakazu Suzuki. 2007. “Hot Spots of Soil Respiration in an Asian Tropical Rainforest.” *Geophysical Research Letters* 34 (8). https://doi.org/10.1029/2007GL029587.
42. Ondier, Joseph, Daniel O. Okach, Onyango C. John, and Dennis O. Otieno. 2020. “Influence of Rainfall Amount and Livestock Grazing on Soil Respiration in a Moist Kenyan Savannah.” *African Journal of Ecology* 58 (1): 92–99.
43. Pan, Connor, Vatsal Patel, Jonathan Gewirtzman, Ian Richardson, Ravish Dubey, Kelly Caylor, Aaron Dollar, and Elizabeth Forbes. 2024. “Fluxbot: The next Generation - Design and Validation of a Wireless, Open-Source Mechatronic CO2 Flux Sensing Chamber.” In *Proceedings of the 7th ACM SIGCAS/SIGCHI Conference on Computing and Sustainable Societies*, 10:85–96. New York, NY, USA: ACM.
44. Paustian, K., O. Andrén, H. H. Janzen, R. Lal, P. Smith, G. Tian, H. Tiessen, M. Van Noordwijk, and P. L. Woomer. 1997. “Agricultural Soils as a Sink to Mitigate CO_2Emissions.” *Soil Use and Management* 13 (s4): 230–44.
45. Paustian, K., J. Lehmann, S. Ogle, D. Reay, G. Robertson, and Pete Smith. 2016. “Climate-Smart Soils.” *Nature* 532 (April): 49–57.
46. Paustian, K., J. Six, E. T. Elliott, and H. W. Hunt. 2000. “Management Options for Reducing CO2 Emissions from Agricultural Soils.” *Biogeochemistry* 48 (1): 147–63.
47. Phillips, S. C., R. K. Varner, and S. Frolking. n.d. “Interannual, Seasonal, and Diel Variation in Soil Respiration Relative to Ecosystem Respiration at a Wetland to Upland Slope at Harvard Forest.” https://doi.org/10.1029/2008JG000858.

48. Premke, Katrin, Katrin Attermeyer, Jürgen Augustin, Alvaro Cabezas, Peter Casper, Detlef Deumlich, Jörg Gelbrecht, et al. 2016. “The Importance of Landscape Diversity for Carbon Fluxes at the Landscape Level: Small-scale Heterogeneity Matters: Importance of Landscape Diversity for Carbon Fluxes at the Landscape Level.” *WIREs. Water* 3 (4): 601–17.
49. Raich, James W., Christopher S. Potter, and Dwipen Bhagawati. 2002. “Interannual Variability in Global Soil Respiration, 1980–94: GLOBAL SOIL RESPIRATION 1980-94.” *Global Change Biology* 8 (8): 800–812.
50. Reinmann, Andrew B., Ian A. Smith, Jonathan R. Thompson, and Lucy R. Hutyra. 2020. “Urbanization and Fragmentation Mediate Temperate Forest Carbon Cycle Response to Climate.” *Environmental Research Letters* 15 (11): 114036.
51. Risch, Anita C., Alan G. Haynes, Matt D. Busse, Flurin Filli, and Martin Schütz. 2013. “The Response of Soil CO2 Fluxes to Progressively Excluding Vertebrate and Invertebrate Herbivores Depends on Ecosystem Type.” *Ecosystems (New York, N.Y.)* 16 (7): 1192–1202.
52. Rodeghiero, Mirco, and Alessandro Cescatti. 2008. “Spatial Variability and Optimal Sampling Strategy of Soil Respiration.” *Forest Ecology and Management* 255 (1): 106–12.
53. Rundel, Philip W., Eric A. Graham, Michael F. Allen, Jason C. Fisher, and Thomas C. Harmon. 2009. “Environmental Sensor Networks in Ecological Research.” *The New Phytologist* 182 (3): 589–607.
54. Saunders, Taylor, Jaron Adkins, Karen H. Beard, Trisha B. Atwood, and Bonnie G. Waring. 2023. “Herbivores Influence Biogeochemical Processes by Altering Litter Quality and Quantity in a Subarctic Wetland.” *Biogeochemistry*, November. https://doi.org/10.1007/s10533-023-01098-9.
55. Savage, K., R. Phillips, and E. Davidson. 2014. “High Temporal Frequency Measurements of Greenhouse Gas Emissions from Soils.” *Biogeosciences* 11 (10): 2709–20.
56. Savage, Kathleen, Eric A. Davidson, Andrew D. Richardson, and David Y. Hollinger. 2009. “Three Scales of Temporal Resolution from Automated Soil Respiration Measurements.” *Agricultural and Forest Meteorology* 149 (11): 2012–21.
57. Savage, Kathleen E., and Eric A. Davidson. 2003. “A Comparison of Manual and Automated Systems for Soil CO2 Flux Measurements: Trade-Offs between Spatial and Temporal Resolution.” *Journal of Experimental Botany* 54 (384): 891–99.
58. Schmitz, Oswald J., Christopher C. Wilmers, Shawn J. Leroux, Christopher E. Doughty, Trisha B. Atwood, Mauro Galetti, Andrew B. Davies, and Scott J. Goetz. 2018. “Animals and the Zoogeochemistry of the Carbon Cycle.” *Science (New York, N.Y.)* 362 (6419): eaar3213.

59. Tang, Jianwu, Dennis D. Baldocchi, and Liukang Xu. 2005. “Tree Photosynthesis Modulates Soil Respiration on a Diurnal Time Scale.” *Global Change Biology* 11 (8): 1298–1304.
60. Vargas, Rodrigo, Mariah S. Carbone, Markus Reichstein, and Dennis D. Baldocchi. 2011. “Frontiers and Challenges in Soil Respiration Research: From Measurements to Model-Data Integration.” *Biogeochemistry* 102 (1–3): 1–13.

Supplementary Information

Assessment of CO_2 Concentration-Dependent Bias in Fluxbot Measurements

Non-dispersive infrared (NDIR) CO_2 sensors may exhibit concentration-dependent measurement artifacts at elevated CO_2 levels due to optical interference or sensor saturation effects. To evaluate potential systematic bias in fluxbot measurements, we conducted a comprehensive comparison between fluxbot flux estimates and concurrent autochamber measurements across the full range of observed starting CO_2 concentrations. We analyzed 5,593 paired flux measurements collected over 30 days (October 2-November 1, 2023) from fluxbot and autochamber systems deployed at Harvard Forest. Data underwent identical quality control procedures: removal of negative flux values and interquartile range filtering to exclude outliers. Starting CO_2 concentrations for fluxbot measurements ranged from 255 to 3,135 ppm (median = 491 ppm).

Measurements were categorized into four concentration ranges: Low (< 450 ppm, n = 673), Normal (450-600 ppm, n = 3,956), Elevated (600-850 ppm, n = 548), and High (≥ 850 ppm, n = 416). Bias was calculated as the difference between fluxbot and autochamber flux estimates, with autochamber data averaged by hour and stand prior to comparison. To distinguish systematic sensor effects from random measurement noise, we applied 3-hour rolling means to the time series and repeated the analysis on temporally smoothed data (n = 5,589 observations). Statistical analysis included Spearman rank correlation between starting CO_2 concentration and bias, linear regression analysis, and assessment of measurement precision (RMSE) and correlation coefficients across concentration ranges.

Overall Bias Characteristics

Analysis of individual measurements revealed a weak but statistically significant correlation between starting CO_2 concentration and measurement bias (Spearman $\rho = 0.062$, $p = 3.56 \times 10^{-6}$). Linear regression indicated a small negative slope of -5.75×10^{-4} bias units per ppm CO_2, with minimal explanatory power ($R^2 = 0.012$). The overall mean bias was -0.182 μmol m^{-2} s^{-1}, representing 6.9% of mean flux magnitude.

Concentration-Dependent Bias Patterns

Bias magnitude and measurement precision varied across concentration ranges:

- **Low concentrations (< 450 ppm):** Mean bias = -0.481 μmol m^{-2} s^{-1} (-19.4% of typical flux), RMSE = 1.07, r = 0.354
- **Normal concentrations (450-600 ppm):** Mean bias = -0.043 μmol m^{-2} s^{-1} (-1.7% of typical flux), RMSE = 1.16, r = 0.304
- **Elevated concentrations (600-850 ppm):** Mean bias = -0.390 μmol m^{-2} s^{-1} (-13.4% of typical flux), RMSE = 1.51, r = 0.296
- **High concentrations (≥ 850 ppm):** Mean bias = -0.744 μmol m^{-2} s^{-1} (-29.3% of typical flux), RMSE = 1.58, r = 0.129

Temporal Smoothing Analysis

Application of 3-hour rolling means fundamentally altered the bias relationship. The correlation between starting CO_2 concentration and bias became non-significant ($\rho = -0.025$, $p = 0.067$), despite a slight increase in explanatory power ($R^2 = 0.014$). Measurement precision improved substantially across all concentration categories, with overall RMSE decreasing from 1.22 to 0.86 μmol m^{-2} s^{-1}. Individual concentration categories showed enhanced fluxbot-autochamber correlations, particularly in the normal range (r = 0.304 to 0.449).

Data Distribution and Statistical Power

The majority of flux measurements (82.8%) occurred at relatively low CO_2 concentrations (< 600 ppm). High-concentration measurements (≥ 850 ppm) comprised 7.4% of the dataset (416 observations), limiting statistical power for assessing sensor performance at extreme CO_2 levels.

Magnitude and Nature of Bias Effects

The concentration-dependent bias detected in individual measurements represents a minor component of overall measurement uncertainty. The temporal smoothing analysis reveals that this bias primarily reflects random measurement variability rather than systematic sensor interference. When short-term noise is removed through 3-hour rolling means, the concentration dependence largely disappears, indicating that the original correlation was driven by temporally-correlated measurement errors rather than consistent sensor artifacts.

Measurement Precision

Individual measurement correlations between fluxbot and autochamber systems decreased with increasing CO_2 concentration ($r = 0.354$ to 0.129), and RMSE increased from 1.07 to 1.58 μmol m^{-2} s^{-1}. However, temporal smoothing dramatically improved precision across all categories, demonstrating that apparent concentration-dependent degradation primarily reflects increased short-term variability rather than systematic sensor malfunction.

Statistical vs. Practical Significance

While the concentration-dependent bias achieves statistical significance in individual measurements ($p < 0.001$), the effect represents minimal practical impact:

1. **Small effect size:** The concentration-dependent bias explains only 1.2% of total bias variance ($R^2 = 0.012$)
2. **Limited temporal consistency:** The relationship becomes non-significant when analyzed with 3-hour temporal smoothing
3. **Minimal bias magnitude:** For the normal concentration range containing 70.7% of all observations, mean bias is only -0.043 μmol m^{-2} s^{-1} (1.7% of typical flux magnitude)
4. **Improved precision with smoothing:** RMSE decreases by 30% when temporal noise is reduced through rolling means

Conclusions

Our analysis confirms the presence of statistically significant concentration-dependent bias in individual fluxbot CO_2 flux measurements. However, temporal smoothing analysis demonstrates that this bias primarily represents random measurement variability rather than systematic sensor interference with measured flux rates, even if there is system sensor interference with absolute concentrations. The small magnitude of bias relative to typical measurement uncertainty, combined with the loss of statistical significance under temporal smoothing, indicates that concentration-dependent effects on measured flux rate do not substantially compromise the scientific utility of fluxbot measurements. The apparent degradation of measurement precision at high CO_2 concentrations reflects increased short-term variability rather than systematic sensor malfunction, as evidenced by substantial precision improvements when temporal noise is reduced through rolling means.

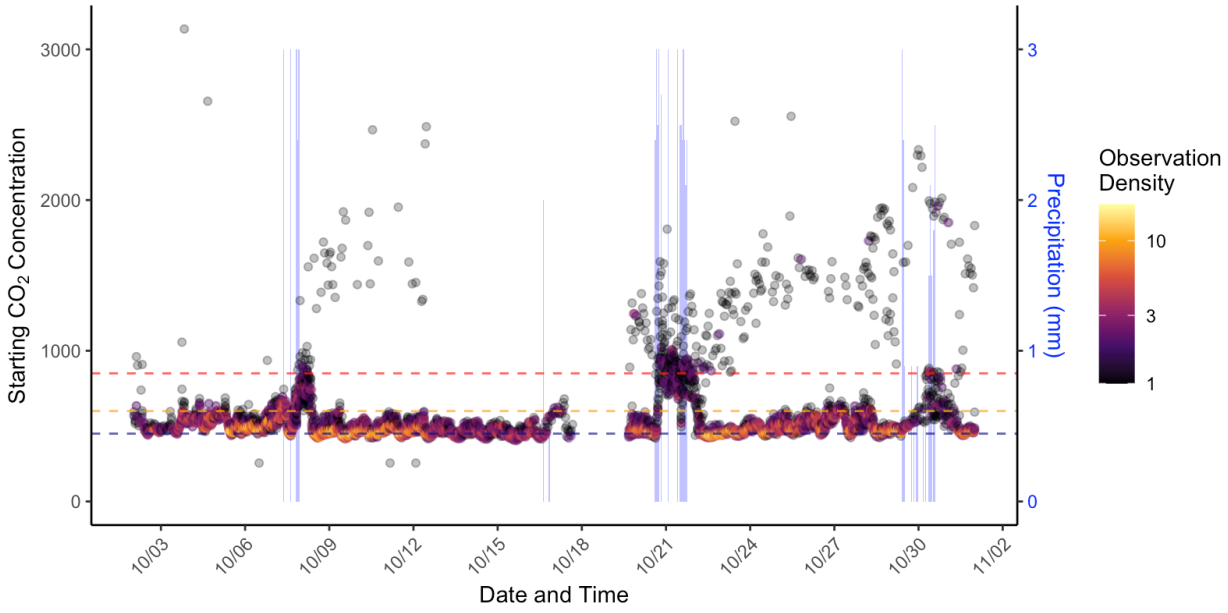

Figure S1. Starting CO_2 concentrations and precipitation during Fluxbot 2.0 deployment at Harvard Forest. Time series showing starting CO_2 concentrations measured by Fluxbot units during chamber closure. Points are colored by local data density, with warmer colors indicating higher observation frequency. Blue bars represent daily precipitation measured at the Fisher Meteorological Station. Horizontal dashed lines indicate concentration thresholds used for bias analysis: 450 ppm (blue, low/normal boundary), 600 ppm (orange, normal/elevated boundary), and 850 ppm (red, elevated/high boundary). The majority of measurements (82.8%) occurred below 600 ppm, with high concentrations (≥850 ppm) comprising 7.4% of observations. Precipitation events show temporal association with periods of elevated starting CO_2 concentrations, reflecting enhanced soil respiration activity and reduced gas exchange between chamber headspace and atmosphere during wet conditions.

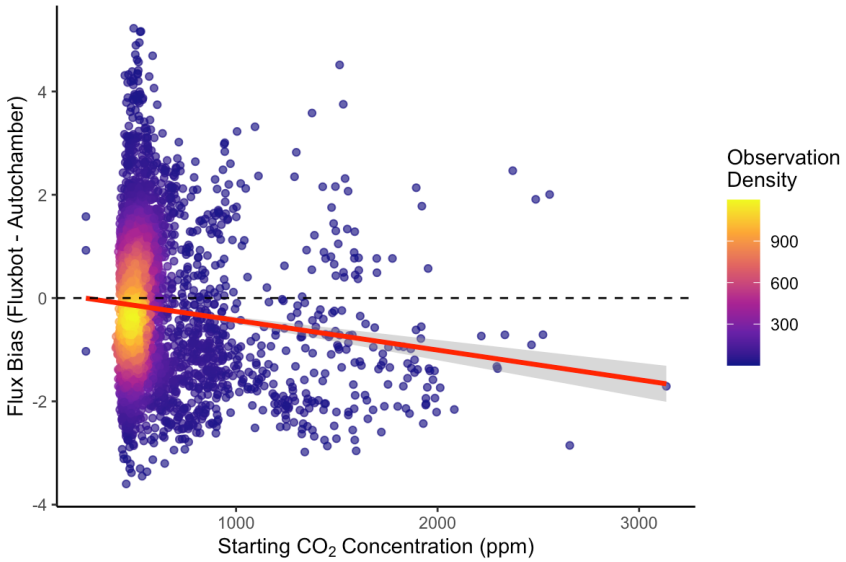

Figure S2. Fluxbot bias as a function of starting CO_2 concentration Scatter plot showing the relationship between starting CO_2 concentration and measurement bias (fluxbot minus autochamber flux estimates). Points are colored by local data density to highlight regions with higher observation frequency. The red regression line shows a statistically significant but weak negative relationship (Spearman $\rho = 0.062$, $p < 0.001$, $R^2 = 0.012$). Data include 5,593 IQR-filtered paired measurements from Harvard Forest (October 2-November 1, 2023). Despite statistical significance, the relationship explains minimal variance in bias.

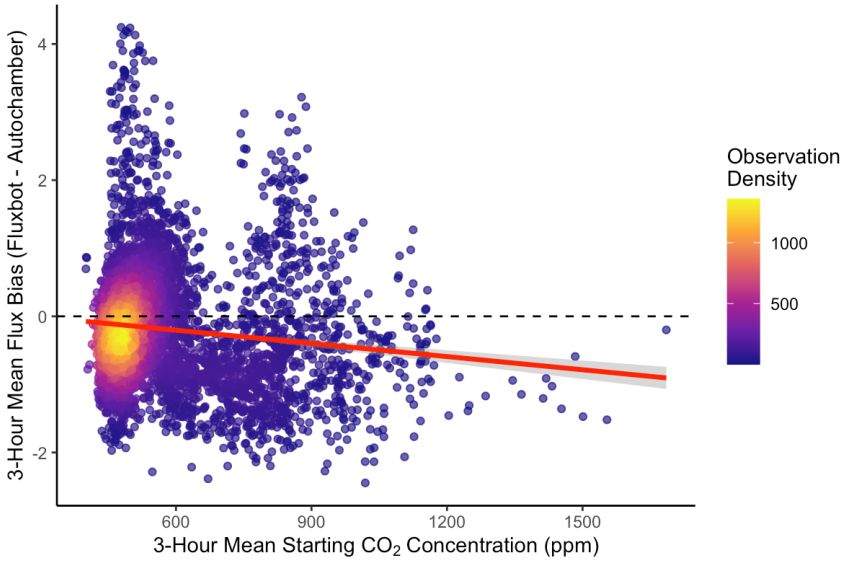

Figure S3. Smoothed fluxbot bias versus starting CO_2 concentration Scatter plot using 3-hour rolling means to reduce short-term measurement noise, comparable to Figure S2. Points are colored by local data density. The regression line shows no significant correlation after temporal smoothing (Spearman $\rho = -0.025$, $p = 0.067$), indicating that the concentration-dependent bias observed in individual measurements primarily reflects random variability rather than systematic sensor interference.

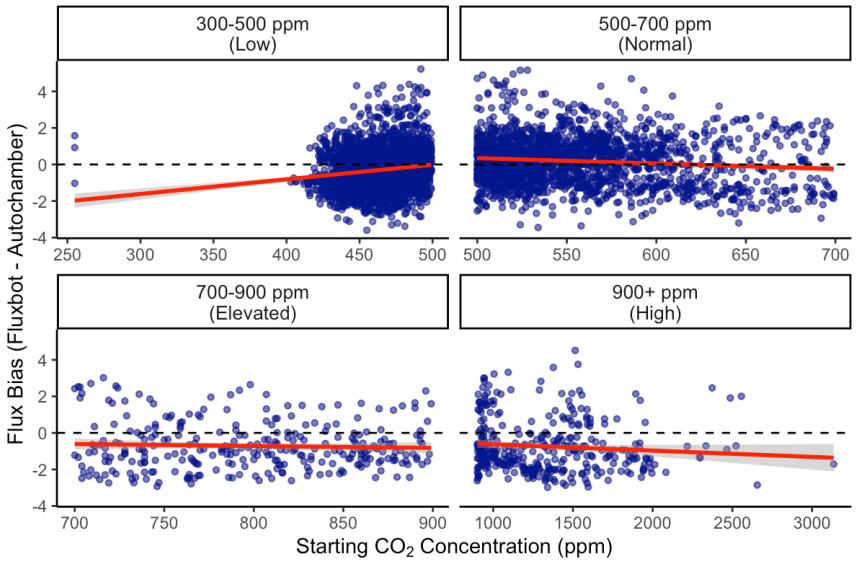

Figure S4. Concentration-dependent bias patterns across measurement ranges Faceted scatter plots showing bias patterns within four CO_2 concentration ranges: 300-500 ppm (Low), 500-700 ppm (Normal), 700-900 ppm (Elevated), and 900+ ppm (High). Each panel displays the relationship between starting CO_2 concentration and flux bias with individual regression lines and 95% confidence intervals. The faceted view reveals heterogeneous patterns across concentration ranges, with most data concentrated in the normal range where bias is minimal.

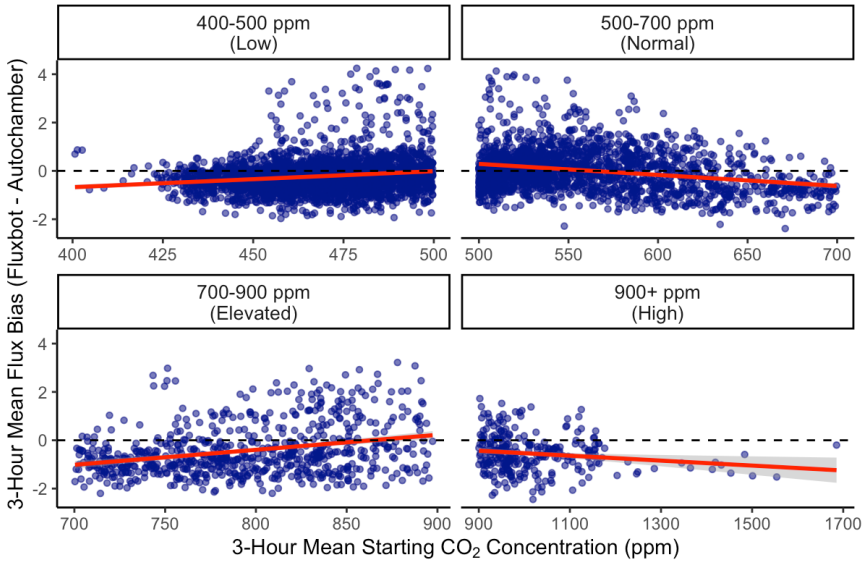

Figure S5. Smoothed bias patterns across concentration ranges Faceted scatter plots using 3-hour rolling mean. The temporal smoothing reveals more stable patterns within each concentration range. Comparison with Figure S4 demonstrates that apparent concentration dependence largely disappears when short-term noise is reduced, supporting the conclusion that observed bias represents measurement variability rather than systematic sensor artifacts.

Table S1. Bias assessment for individual fluxbot measurements compared to concurrent autochamber flux estimates across CO_2 concentration ranges. Fluxbot and autochamber data underwent identical quality control (negative flux removal and IQR filtering). Autochamber measurements were averaged by hour and stand prior to comparison. Bias calculated as fluxbot minus autochamber flux estimates, with negative values indicating fluxbot underestimation. Spearman correlation (ρ) and R^2 values represent the relationship between starting CO_2 concentration and measurement bias. Correlation (r) represents agreement between fluxbot and autochamber flux estimates within each concentration category (n = 5,593 paired observations).

Concentration Range	N Observations	Percent of Data	Mean Bias (μmol m^{-2} s^{-1})	RMSE	Correlation (r)	Bias (% of Flux)
Low (< 450 ppm)	673	12.0%	-0.481	1.072	0.354	-19.4%
Normal (450-600 ppm)	3,956	70.7%	-0.043	1.160	0.304	-1.7%
Elevated (600-850 ppm)	548	9.8%	-0.390	1.507	0.296	-13.4%
High (≥ 850 ppm)	416	7.4%	-0.744	1.583	0.129	-29.3%
Overall	**5,593**	**100.0%**	**-0.182**	**1.224**	**0.293**	**6.9%**

Table S2. Bias assessment for temporally smoothed fluxbot measurements using 3-hour rolling means compared to similarly smoothed autochamber flux estimates. Concentration categories based on 3-hour mean starting CO_2 values. Spearman correlation (ρ) and R^2 represent the relationship between 3-hour mean starting CO_2 concentration and 3-hour mean measurement bias. Correlation (r) represents agreement between smoothed fluxbot and autochamber flux estimates within each concentration category.

Concentration Range	N Observations	Percent of Data	Mean Bias (μmol m^{-2} s^{-1})	RMSE	Correlation (r)	Bias (% of Flux)
Low (< 450 ppm)	479	8.6%	-0.381	0.581	0.643	-15.4%
Normal (450-600 ppm)	3,750	67.1%	-0.057	0.814	0.449	-2.2%
Elevated (600-850 ppm)	968	17.3%	-0.491	1.039	0.376	-18.8%
High (≥ 850 ppm)	392	7.0%	-0.369	1.057	0.095	-14.5%
Overall	**5,589**	**100.0%**	**-0.182**	**0.860**	**0.418**	**6.9%**

Table S3. Comparison of concentration-dependent bias relationships between individual measurements and 3-hour rolling means. Spearman correlation (ρ) and R^2 quantify the relationship between starting CO_2 concentration and measurement bias (fluxbot minus autochamber). RMSE represents the root mean square error between fluxbot and autochamber flux estimates, with lower values indicating better measurement precision.

Metric	Individual Measurements	3-Hour Rolling Means
Spearman correlation (ρ)	0.062*	-0.025
P-value	3.56×10^{-6}	0.067
R^2	0.012	0.014
Overall RMSE	1.224	0.860

*Statistically significant ($p < 0.05$)

Figure S1. Daily flux measurements retained after quality control across Fluxbot 2.0 and autochamber systems during October 2023 deployment. Each point represents the number of soil CO_2 flux measurements from individual units that passed quality control procedures (negative flux removal and interquartile range filtering) on each day of the 30-day field comparison at Harvard Forest. Point color indicates measurement count, with warmer colors representing higher daily data collection. Fluxbot 2.0 units operated autonomously on hourly measurement cycles, while autochamber units measured every 30 minutes via multiplexed sampling to a central IRGA system. The visualization demonstrates system reliability and data availability patterns that contributed to the final analysis dataset used for validating Fluxbot 2.0 performance against established autochamber measurements. Both systems maintained >95% data retention rates after quality control, with the distributed Fluxbot array showing resilience to localized failures while autochambers achieved slightly higher overall collection efficiency.